Mon. Not. R. Astron. Soc. **310**, 982–1001 (1999)

UBVI CCD photometry of M11 – II. New photometry and surface density profiles

Hwankyung Sung,[1,2★] M. S. Bessell,[3★] Hee-Won Lee,[4★] Yong Hee Kang[2] and See-Woo Lee[5]

[1]*Bohyun-san Optical Astronomy Observatory, Youngcheon, Kyungpook 770-820, Korea*
[2]*Department of Earth Science Education, Kyungpook National University, Taegu 702-701, Korea*
[3]*Research School of Astronomy & Astrophysics, The Australian National University, Private Bag, Weston Creek PO, ACT 2611, Australia*
[4]*Department of Astronomy and Atmospheric Sciences, Kyungpook National University, Taegu 702-701, Korea*
[5]*Department of Astronomy, Seoul National University, Seoul 151-742, Korea*

Accepted 1999 July 7. Received 1999 June 18; in original form 1999 April 7

ABSTRACT

Extensive *UBVI* CCD photometry has been obtained for the intermediate-age open cluster M11 (NGC 6705). From this new photometry we derive the cluster parameters [$V_0 - M_V = 11.55 \pm 0.10$, $E(B-V) = 0.428 \pm 0.027$ and radius = 16 arcmin] and age ($\log t_{\rm age} = 8.4 \pm 0.1$). We also derive density profiles and confirm the mass segregation in M11. The slope of the mass function increases systematically with increasing radius from the centre. We also confirm the existence of main-sequence field stars having similar photometric characteristics to M11. A large population of field red giant stars is also found in the observed fields.

Key words: stars: evolution – Hertzsprung–Russell (HR) diagram – stars: luminosity function, mass function – open clusters and associations: individual: M11 (NGC 6705).

1 INTRODUCTION

Studies of intermediate-age open clusters can provide much information on the stellar evolution of intermediate-mass stars (Harris 1976; Schmidt 1984; Sowell 1987; Sung & Bessell 1999) as well as the dynamical evolution of clusters (Mathieu 1984; Sung et al. 1996, hereafter Paper I; Perryman et al. 1998). However, quantitative comparisons between theory and observations of these open clusters suffer from several difficulties. First, most open clusters in the Galaxy are located in the Galactic plane, and therefore their photometric quantities are greatly affected by obscuring material. Secondly, in such regions many field interlopers are expected. Membership selection is therefore of crucial importance in the study of open clusters. Colour–magnitude (CM) diagrams are a very useful tool in selecting members, but in some cases CM diagrams alone cannot give a definite result. In those cases, other independent criteria, such as proper motion studies or radial velocity surveys, are required, although these kinematic data are usually limited to bright stars only. Thirdly, because most open clusters have only a small number of members, statistically significant conclusions on stellar evolution or on dynamical evolution are difficult to obtain.

Recently, Raboud & Mermilliod (1998a,b) showed mass segregation in two nearby intermediate-age open clusters, the Pleiades and Praesepe, using all available photometric, proper motion data as well as their own extensive radial velocity survey data. The results clearly showed that the radial distribution of massive, multiple stars is different from that of low-mass single stars. The mass function of the inner region also differed from that of the outer. Raboud & Mermilliod also found mass segregation of massive stars in the young open cluster NGC 6231, which is younger than the typical relaxation time-scale of open clusters ($\tau_{\rm relax} \sim 10^7$ yr), and discussed the implications of mass segregation in young open clusters in relation to star formation processes (see also Sagar et al. 1988).

M11 is one of a few open clusters well suited for the study of dynamical evolution as well as stellar evolution, but it has not been observed much. M11 has a large number of members, including about 30 core He-burning red giants; its Trumpler type is I 2r with a very good central concentration. Johnson, Sandage & Wahlquist (1956) performed *UBV* photoelectric and photographic photometry for about 400 stars in the cluster field. McNamara, Pratt & Sanders (1977, hereafter MPS) presented proper motion membership probabilities for a $\sim 20 \times 20$ arcmin^2 region of M11 down to $V \approx 16$. Later, McNamara & Sanders (1977) studied the internal motions of stars in M11. They found a velocity dispersion of 2.9 km s^{-1} independent of stellar mass and the existence of an extensive halo. They suggested that energy equipartition is not present in the cluster. Solomon & McNamara (1980) performed *BV* photographic photometry and confirmed the existence of an extensive halo.

★ E-mail: sungh@boao.ke.kr (HS); bessell@mso.anu.edu.au (MSB); hwlee@vega.kyungpook.ac.kr (H-WL); yhkang@kyungpook.ac.kr (YHK)

Mathieu (1984) performed deep photographic photometry and star counts using Kitt Peak National Observatory (KPNO) 4-m plates. He also presented a discussion on cluster membership and the reliability of proper motion studies. He considers a star to be a member if its position in the CM diagram is consistent with that of a main-sequence (MS) star in the cluster even if its proper motion membership probability is very low (down to $P_\mu = 0.1$). He presented the surface density profile out to $r \sim 9.6$ arcmin and compared it with the results from dynamical evolution models. He also found a slight deficiency of low-mass stars in the luminosity function even after correcting for the incompleteness of the proper motion data. On the other hand, Brocato, Castellani & DiGiorgio (1993) found a factor of 2.5 enhancement of lower ($V \geq 15$) MS stars from *BV* CCD photometry of a 5×5 arcmin^2 field centred about 7 arcmin west of the cluster centre using the European Southern Observatory (ESO) 3.6-m telescope. Sung et al. (1996) attributed this enhancement of MS stars to field star contamination.

Mathieu et al. (1986) presented precise radial velocities for 39 stars in M11, deriving a mean radial velocity of 34.5 ± 1.4 km s^{-1}. Amongst 33 proper motion members ($P_\mu \geq 0.5$), they found two

Table 1. Observation summary.

Object	Region	Date of Obs.	Exposure time (s)	FWHM ($''$)[a]	Standard star	Remark
	CS	1996 Aug 24	*I*:5; *V*:5; *B*:10; *U* : 300 × 2	1.9	Landolt	photometric
	CS	1996 Aug 25	*I*:20; *V*:50; *B*:100; *U*:300	1.5	Landolt	photometric
	CN	1997 Jun 5	*I*:5, 60; *V*:5, 120; *B*:10, 300; *U*:30, 600	2.3	SAAO	cloud
M11	SE	1997 Jun 23	*I*:5, 60; *V*:5, 120; *B*:10, 300; *U*:30, 600	2.5	SAAO	photometric
	SW	1997 Jun 23	*I*:5, 60; *V*:5, 120; *B*:10, 300; *U*:30, 600	2.5	SAAO	photometric
	NW	1997 Jun 23	*I*:5, 60; *V*:5, 120; *B*:10, 300; *U*:30, 600	2.5	SAAO	photometric
	NE	1997 Jun 23	*I*:5, 60; *V*:5, 120; *B*:10, 300; *U*:30, 600	2.5	SAAO	photometric
	CT	1997 Aug 10	*I*:30; *V*:60; *B*:150; *U*:300	1.9	SAAO	photometric
PN G027.4−03.5		1996 Aug 24	*I*:20; *V*:50; *B*:100; *U*:300	4.0	Landolt	photometric
		1996 Aug 25	*I*:20; *V*:50; *B*:100; *U*:300	1.6	Landolt	photometric

[a] FWHM of long-exposure *V* images.

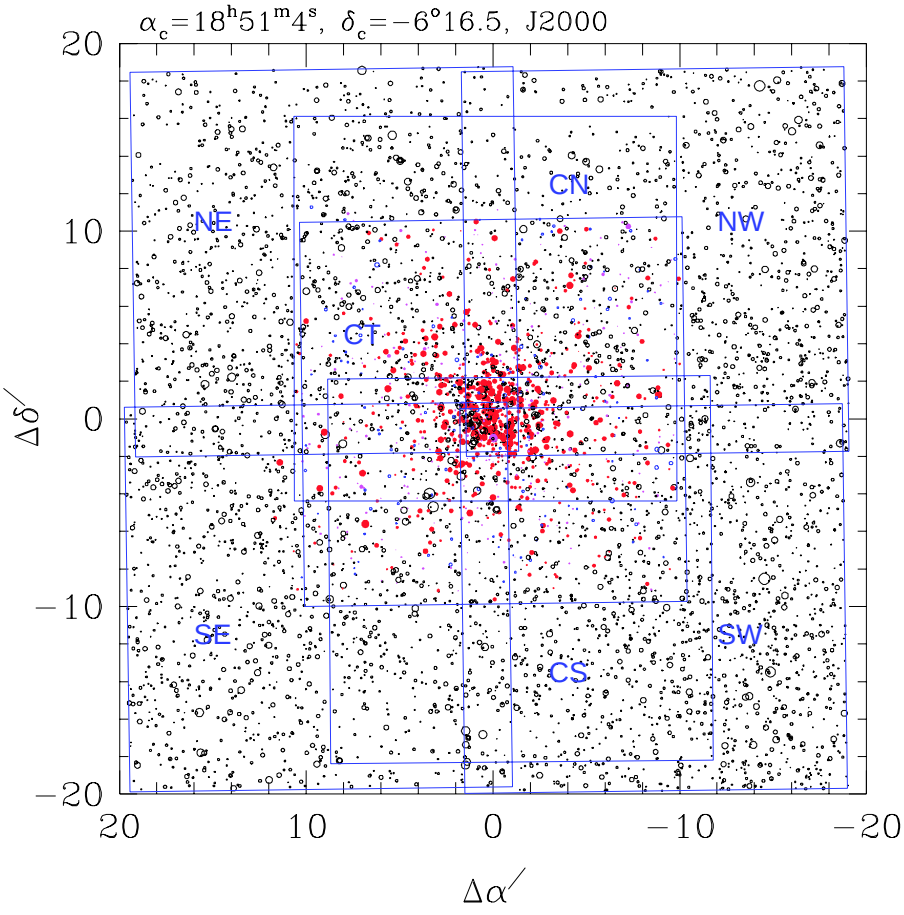

Figure 1. Finding chart for M11. The sizes of the circles are proportional to the magnitudes of the stars. The filled circles represent the proper motion members ($P_\mu \geq 0.7$ in red, ≥ 0.5 in magenta) from MPS. The boxes in the chart represent the observed regions. The names of the observed regions are also marked.

spectroscopic binaries. Later, Lee, Mathieu & Latham (1989) determined the eccentricity and period of these binaries and, using the revised Yale isochrones of age 150 Myr, they derived a lower limit to the distance modulus, $m - M = 12.7$ (the best fit is 12.8).

Recently Sung et al. (1996) performed a statistical analysis for M11 using SITe 2048 × 2048 CCD images. They derived a radius ($r \sim 10$ arcmin) for the cluster and confirmed the radial variation of the luminosity function together with that of the CM diagram morphology. In addition, they proposed the existence of field MS stars overlying the MS band of M11. This was not a definitive study, however, as they observed only the central region ($r \sim 12$ arcmin) and the quality of their data was diminished owing to the large readout noise of the CCD.

As noted above, M11 is a rich cluster well suited for studying dynamical evolution. In common with other intermediate-age open clusters, its age ($\tau_{\rm age} = 2 \times 10^8$ yr: Mathieu 1984) is greater than the relaxation time-scale ($\tau_{\rm relax} = 4 \times 10^7$–$1.3 \times 10^8$ yr: Mathieu 1984) and far greater than the cluster crossing time. In any study of cluster dynamics, homogeneous and complete photometric data are very important. For M11 this is complicated by claims that the cluster has an extended halo (McNamara & Sanders 1977; Solomon & McNamara 1980) and by the fact that, being located near the Scutum star cloud, many foreground and/or background field stars are expected to be present. The main purpose of this study is to present new extensive photometric data for M11. Using these new data, we will derive the surface density profile of the cluster, which, without kinematic information, is the only interface with the dynamics of the cluster.

In Section 2 we will summarize our extensive CCD observations of M11 and one region in the Scutum star cloud (PN G027.4−03.5), and show the existence of several groups of stars in the observed field. In Section 3 some fundamental parameters, such as interstellar reddening $E(B - V)$, distance modulus, radius and age, will be derived. In Section 4 the surface density profile of M11 will be derived. In the statistical analysis of crowded regions, the completeness of data is very important. To check for completeness, we have constructed a model cluster using the observed surface density profile and a Monte Carlo technique. The result of this completeness test will be discussed in Section 4. The radial variation of the luminosity and mass functions will also be derived. In Section 5 a discussion of the red giant population will be presented. Section 6 is the summary.

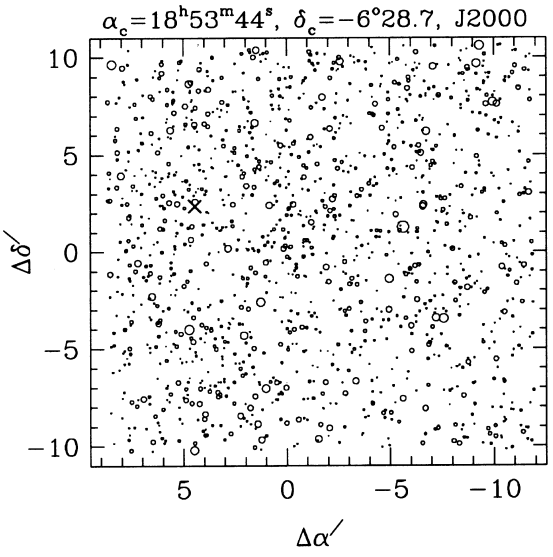

Figure 2. Finding chart for the Scutum star cloud (PN G027.4−03.5). The cross in the figure represents the position of PN G027.4−03.5. The others symbols are the same as for Fig. 1.

2 OBSERVATIONS

UBVI CCD photometry was performed for the whole area of M11 during observing runs from 1996 August to 1997 August at Siding Spring Observatory with the 40-inch telescope (*f*/8) and thinned SITe 2048 × 2048 CCD (24-μm pixels). The scale was 0.602 arcsec pixel^{-1}, giving 20.5 arcmin on a side. The summary of the observations is presented in Table 1, and a finding chart for the observed area is shown in Fig. 1. The names of the regions are also marked in the figure. The filled circles in the central region represent the proper motion members ($P_\mu \geq 0.5$) from MPS. To obtain information on the field star population, we observed a region around PN G027.4−03.5 which is about 40 arcmin away from the M11 centre. The finding chart for PN G027.4−03.5 is presented in Fig. 2. The cross in Fig. 2 represents the position of PN G027.4−03.5.

All the pre-processing was done using the IRAF/CCDRED package. Instrumental magnitudes were obtained with the IRAF version of DAOPHOT II (Stetson 1991) via point spread function (PSF) fitting. During the 1996 August observing run, we observed the Landolt standards (SA 110, Mark A and T Phe regions). In the transformation of *U* magnitudes, a non-linear term was involved (see Sung, Bessell & Lee 1998). To minimize such a non-linear term, we used for later *U* observations an additional UG1 1-mm filter; we also observed South African Astronomical Observatory (SAAO) E-region standards (E5 and E7 in 1997 June, and E6 and E7 in 1997 August). The mean values of the transformation coefficients were derived from observations (1997 June, August and November observing runs) of SAAO E-region standards (Menzies et al. 1989), SAAO observations of equatorial standards (Menzies et al. 1991) and Supplementary southern standards for $UBV(RI)_C$ photometry (Kilkenny et al. 1998). The primary extinction coefficients were determined every night, but for the secondary extinction coefficients we used the mean values adopted previously (Sung et al. 1998). In the transformation of the data on 1997 June 5, the extinction coefficients for the first half for the night were used. All the data are consistent within 0.02 mag in *V*, $(V - I)$ and $(B - V)$, and 0.03 mag in $(U - B)$, except for the data obtained in 1996 August which showed a large difference in $(U - B)$. Such a difference may have been caused by the non-linear transformation to the standard systems (see Menzies et al. 1991 or Bessell 1995). To avoid systematic errors resulting from the use of data observed with different *U* instrumental systems and transformed to different standard systems, we decided not to use the data observed during the 1996 August observing run (field CS). However, the control field (PN G027.4−03.5) was only observed during the 1996 August run. We have used those data to estimate the field star population, and luckily the difference in $(U - B)$ is not a critical problem for that study. During the 1996 observing run, the moonlight was very bright and therefore the limiting magnitude was about 1 mag brighter than during other runs.

We measured a total of 166 491 stars brighter than $V = 21$. Photometric data for 14 179 stars brighter than $V = 17$ are presented in Table 2. Table 2 lists the ID number, $\Delta\alpha(')$, $\Delta\delta(')$

Table 2. Photometric data for M11. The full table is available electronically.

ID	$\Delta\alpha(')$	$\Delta\delta(')$	V	$V-I$	$B-V$	$U-B$	ϵ_V	ϵ_{V-I}	ϵ_{B-V}	ϵ_{U-B}	$n_{\rm obs}$				MPS	P_μ	SZT	P_μ
7011	−0.935	−16.153	15.925	1.279	1.114	0.732	0.019	0.001	0.004	0.021	4	4	4	3				
7012	−0.934	−1.935	16.088	2.082	1.054	…	0.011	0.027	0.896	…	7	7	5					
7013	−0.933	2.488	15.473	1.071	0.848	0.358	0.001	0.010	0.006	0.002	7	7	7	7	1254	0.40		
7014	−0.930	2.659	14.339	0.570	0.456	0.305	0.008	0.008	0.011	0.015	7	7	7	7	1252	0.99	619	1.00
7015	−0.930	−16.648	16.103	1.938	1.812	2.040	0.015	0.002	0.007	0.288	4	4	4	1				

$\alpha_c = 18^h51^m4^s$, $\delta_c = -6°16'.5$, J2000.0.

Table 3. Photometric data for PN G027.4−03.5. The full table is available electronically.

ID	$\Delta\alpha$	$\Delta\delta$	V	$V-I$	$B-V$	$U-B$	ϵ_V	ϵ_{V-I}	ϵ_{B-V}	ϵ_{U-B}	$n_{\rm obs}$			
1	−11.924	−6.975	16.235	1.094	0.874	…	0.005	0.027	0.050	…	2	2	1	
2	−11.903	−7.151	15.067	1.880	1.682	…	0.026	0.011	0.025	…	2	2	1	
3	−11.892	−8.323	16.663	1.922	1.693	…	0.100	0.065	0.150	…	2	2	2	
4	−11.870	−6.670	16.959	1.098	0.829	0.153	0.021	0.042	0.072	0.164	2	2	2	1
5	−11.867	−9.905	16.464	1.143	0.908	0.305	0.028	0.042	0.051	0.109	1	1	1	1

$\alpha_c = 18^h53^m44^s$, $\delta_c = -6°28'.7$, J2000.0.

Table 4. Mean photometric errors.

V	M11 (NGC 6705)				PN G027.4−03.5			
	ϵ_V	ϵ_{V-I}	ϵ_{B-V}	ϵ_{U-B}	ϵ_V	ϵ_{V-I}	ϵ_{B-V}	ϵ_{U-B}
10–11	0.010	0.013	0.009	0.014	0.002	0.003	0.004	0.004
11–12	0.011	0.013	0.011	0.014	0.006	0.006	0.005	0.009
12–13	0.006	0.007	0.006	0.015	0.006	0.005	0.005	0.016
13–14	0.009	0.010	0.011	0.024	0.008	0.008	0.009	0.040
14–15	0.010	0.014	0.012	0.050	0.011	0.012	0.014	0.076
15–16	0.012	0.016	0.020	0.086	0.020	0.021	0.026	0.138
16–17	0.016	0.023	0.034	0.124	0.037	0.040	0.052	0.191
17–18	0.028	0.037	0.068	0.173	0.071	0.079	0.109	0.245
18–19	0.056	0.070	0.129	0.247	0.119	0.151	0.283	0.381
19–20	0.105	0.126	0.213	0.338	…	…	…	…

Table 5. Comparison with photoelectric photometry.

Author	ΔV	$\Delta(B-V)$	$\Delta(U-B)$	n
Johnson et al. (1956)	−0.022 ± 0.048	+0.007 ± 0.020	−0.021 ± 0.020	20
Eggen (1974)	+0.018 ± 0.104	+0.001 ± 0.038	+0.001 ± 0.083	17
Stetson & Harris (1988)	+0.001 ± 0.028	−0.003 ± 0.029	…	29

relative to the eye-estimated cluster centre ($\alpha = 18^h51^m4^s$, $\delta = -6°16'.5$, J2000.0), the weighted mean values of the magnitude and colour, their errors and the number of independent measurements. The star numbers and proper motion membership probabilities from MPS and Su, Zhao & Tian (1998) are given in the last four columns. The photometric data for the PN G027.4−03.5 region are also presented, in Table 3. The full versions of Tables 2 and 3 are available on Synergy and, in machine-readable form, on the Astronomical Data Center (ADC) web site (http://adc.gsfc.nasa.gov/). The full data set for Table 2 is also available on the WEBDA open cluster data base maintained by J.-C. Mermilliod at the University of Lausanne (http://obswww.unige.ch/webda/). We also performed aperture photometry of PN G027.4−03.5. The magnitudes and colours in the Landolt version of the *UBVI* system are $V = 13.55(\pm0.03)$, $(V-I) = -0.51(\pm0.02)$, $(B-V) = 0.73(\pm0.01)$ and $(U-B) = -0.33(\pm0.03)$.

The mean values of the errors in magnitude and colour are listed in Table 4. The *UBV* magnitude and colours for $V_{\rm CCD} \leq 14$ are compared with previous photometry in Table 5, showing differences in the sense of photoelectric minus CCD magnitude. The photometric data of Stetson & Harris (1988) were obtained from CCD images measured to simulate photoelectric photometry. Our new photometry is in good agreement with the zero-points of all other photometry, but the Eggen (1974) data show large scatter in V and $(U-B)$.

3 PHOTOMETRIC DIAGRAMS AND OBSERVATIONAL QUANTITIES

3.1 Photometric diagrams

We have plotted several CM diagrams from our photometry in Fig. 3. The reddened (see Section 3.2) zero-age main-sequence (ZAMS) lines are also plotted. The adopted ZAMS relation in Fig. 3 is mainly from Mermilliod (1981), supplemented by the data of Blaauw (1963) and Schmidt-Kaler (1982). The $(V-I, M_V)$ relation of Sung & Bessell (1999) for bright stars and Cousins' (1978) MS relation between $(B-V)$ and $(V-I)$ were used in the ZAMS M_V versus $(V-I)$ relation. Proper motion members

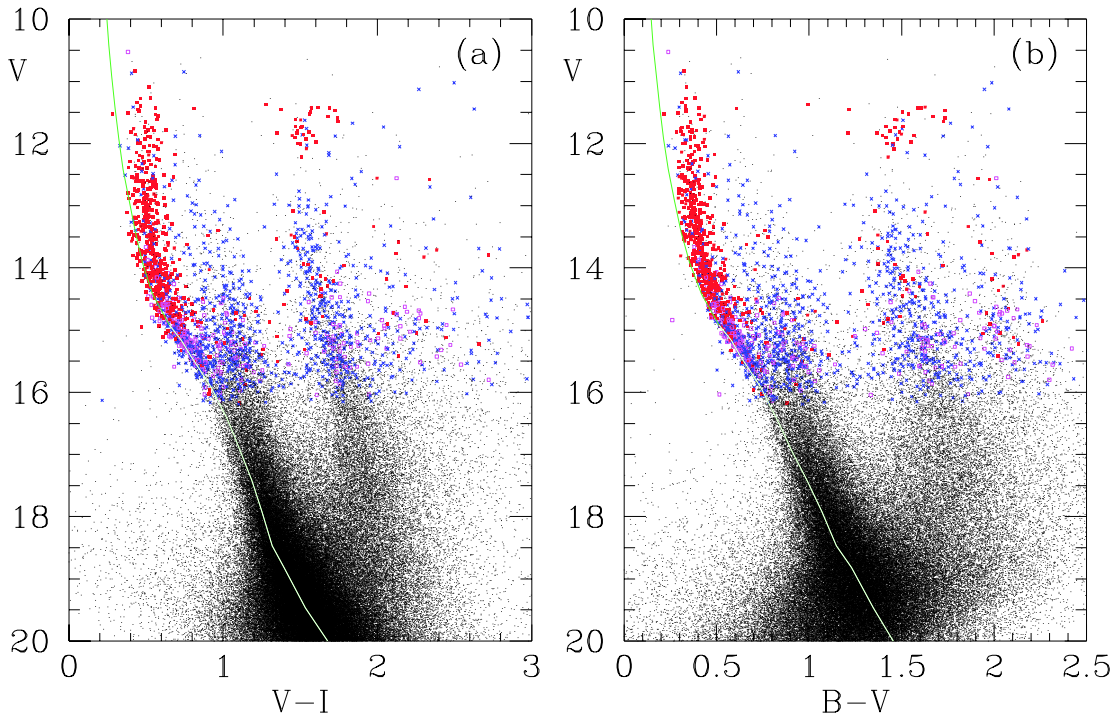

Figure 3. CM diagrams for M11. The thin line represents the reddened ZAMS relation. The filled squares (in red), open squares (in magenta) and crosses (in blue) represent respectively proper motion members ($P_\mu \geq 0.7$), probable members ($0.7 > P_\mu \geq 0.5$) and non-members ($P_\mu < 0.5$). The dots denote stars without proper motion membership probabilities.

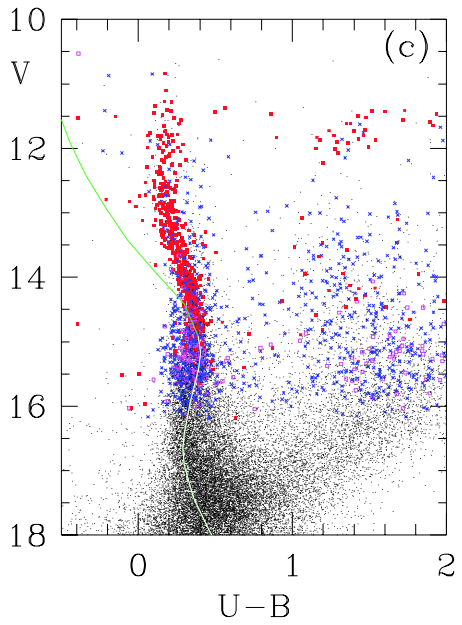

Figure 3 – *continued*

($P_\mu \geq 0.7$: filled squares), probable members ($0.7 > P_\mu \geq 0.5$: open squares) and non-members ($P_\mu < 0.5$: crosses) from MPS are marked in the figures. Proper motion members in Figs 3(a) and (b) constitute a well-defined MS band and a red giant branch. With regard to the faint stars ($V > 14.5$), most of the stars in the MS band of M11 have lower proper motion membership probabilities, while the fraction of proper motion members in the red part (i.e. field interlopers) has increased. This means that the proper motion membership probability is a function of magnitude, and therefore the proper motion study by MPS must be less reliable for the faint stars. Su et al. (1998) also performed a proper motion study for the cluster and corrected for the spatial and magnitude dependence of the proper motion, but their study was limited to the bright stars only. In addition, many faint field giants ($V \geq 12.3$) and intermediate population stars ($V - I = 0.8$–1.0) were classified as proper motion members.

In Fig. 4, we present the ($B - V$, $U - B$) and ($V - I$, $(B - V) - (V - I)$) diagrams for bright stars [$V \leq 16$ in (a) and $V \leq 17$ in (b)]. The MS stars in M11 ($B - V \leq 0.6$) do not show any noticeable UV excess, which implies that the abundance of M11 is near solar. This is consistent with the abundance determination by Twarog, Ashman & Anthony-Twarog (1997: $[\mathrm{Fe/H}]_{\mathrm{NGC\,6705}} = 0.136 \pm 0.086$ using six stars in M11).

There are three distinct branches that can be seen in Figs 3(a) and (b). The first and bluest branch comprises the MS stars of M11. One point worth noticing is that there are several proper motion non-member stars even in the MS band of M11. Such stars can be found in the CM diagrams of the outer regions (see Fig. 7) as well as in the CM diagram of the PN G027.4−03.5 region (see Fig. 5) or even in the CM diagrams of other regions in the Sgr–Car arm (see fig. 3 of Sung et al. 1998). They are bona fide field MS stars in the Sgr–Car arm. Sung et al. (1996) already noted the existence of such a population in the M11 field (cf. the membership criteria of Mathieu 1984). The second branch comprises the intermediate population between the MS band and the red giants. Most of these stars are proper motion non-members and therefore field stars. In Fig. 4(a) we can easily see that the stars in this second branch ($B - V = 0.6$–1.1) are less reddened F- and G-type MS stars. The third and very distinctive branch is the red star population with ($V - I$) = 1.5–2.1. The

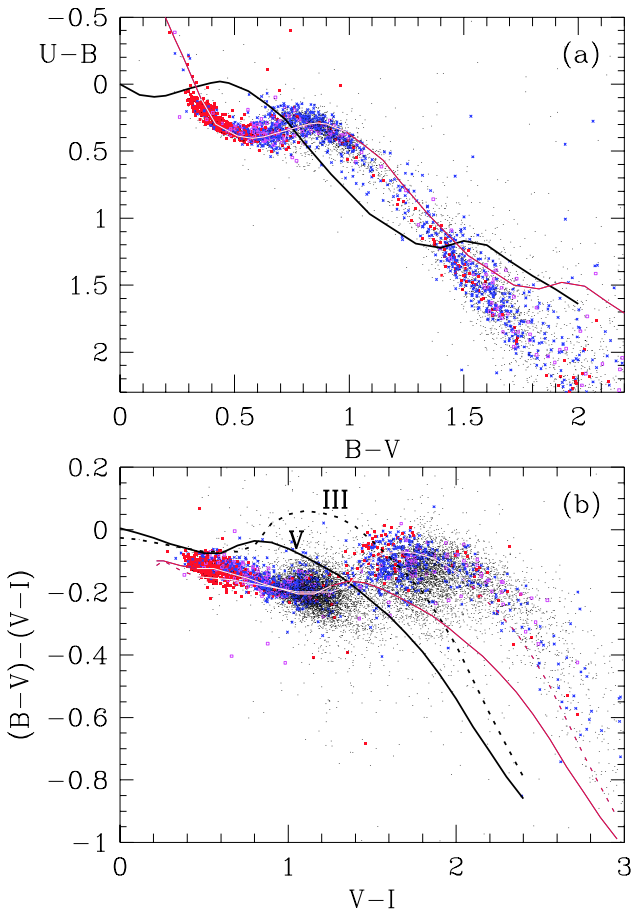

Figure 4. Colour–colour diagrams for M11. (a) $(U-B)$ versus $(B-V)$ diagram for $V \leq 16$. (b) $(B-V)$ versus $(V-I)$ diagram for $V \leq 17$. All symbols are the same as in Fig. 3. The dotted lines in (b) represent the unreddened and reddened relations for giant stars, while the solid lines denote those for MS stars.

cluster giants are mostly brighter than $V = 12.5$, but there is a very unusual component fainter than $V = 12.5$. Their corresponding position in the colour–colour diagrams of Fig. 4(b) overlies the brighter M11 red giants, which implies that they are also red giant stars rather than more reddened hot stars or foreground red dwarfs. However, the slope of the 'branch' that they form is not what one would expect for red giants which become redder with increased luminosity, not bluer as seen here. A more detailed discussion on the nature of this red star population is presented in Section 4.1. We have also plotted the CM diagrams and colour–colour diagrams for the PN G027.4−03.5 region in Figs 5 and 6. The overall morphology of Fig. 5 is very similar to that of the outer regions of M11 (see Fig. 7).

A star cluster is a dynamical system, and hence stars in the cluster are subject to dynamical evolution. As a result (due to the tendency towards kinetic energy equipartition), mass segregation will occur in the cluster. To see this effect, we have plotted several $(V-I, V)$ CM diagrams at various radii in Fig. 7. In the figure, we can clearly see drastic changes in the CM diagram morphology as the radius from the cluster centre increases. In the CM diagrams from the inner rings, cluster MS stars and giants dominate the field population. The proportion of the field population increases as the radius increases. At $r > 6$ arcmin, the field star population dominates the cluster MS. As noted above, a non-negligible number of stars coincident with the cluster MS band can be seen even in the field region ($r > 16$ arcmin: see Section 3.3). Such MS stars are also seen even in the Scutum star cloud.

3.2 Reddening and distance

The interstellar reddening $E(B-V)$ of M11 was estimated using the intrinsic colour relation of Mermilliod (1981). The $E(B-V)$ of bright proper motion members ($P_\mu \geq 0.7$) shows a somewhat large scatter [$E(B-V) = 0.38$–0.48]. The mean value of $E(B-V)$ from 297 stars is 0.428 ± 0.027. There is no systematic variation across the cluster field, however, indicating that there is no evident differential reddening across the cluster. Such a large scatter may

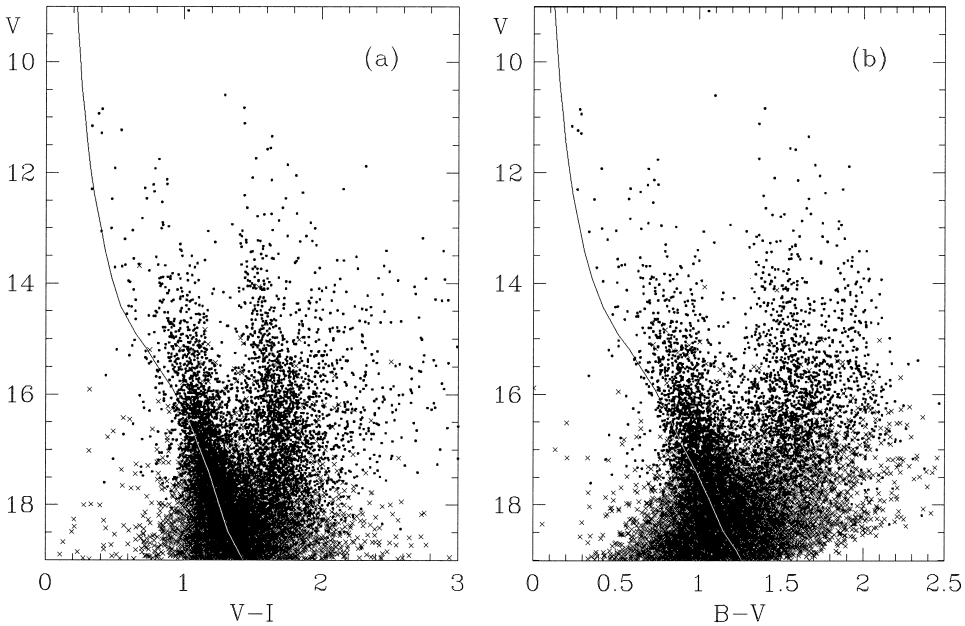

Figure 5. CM diagrams for the PN G027.4−03.5 region. The dots and crosses denote stars with good photometry ($\epsilon \leq 0.1$) and bad-quality photometry ($\epsilon > 0.1$) respectively.

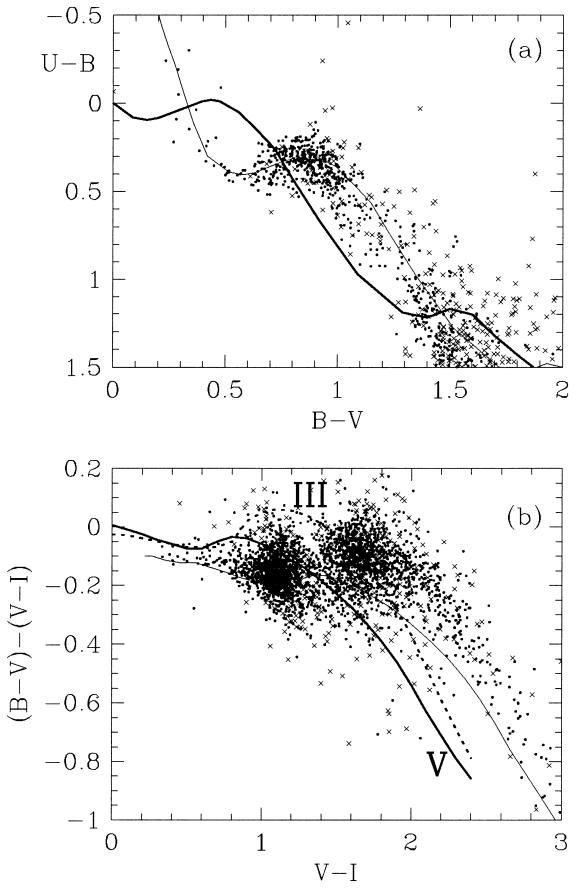

Figure 6. Colour–colour diagrams for the PN G027.4−03.5 region. The symbols are the same as in Fig. 5, and the limiting magnitudes are the same as in Fig. 4. The lines are the same as in Fig. 4.

be caused by other effects, such as chemical peculiarity, photometric error, the Be phenomenon, binarity, inclusion of field interlopers, or the combined effect of all of these. We will use the mean value of $E(B-V)$ in the analysis.

The total-to-selective extinction ratio can be estimated from the colour excess ratio between $(B-V)$ and $(V-I)$ (Guetter & Vrba 1989). The intrinsic colour relation between $(B-V)$ and $(V-I)$ of Sung & Bessell (1999) was used in the $E(V-I)$ estimate. The mean value of $E(V-I)/E(B-V)$ is 1.302 ± 0.052. The total-to-selective extinction ratio $R[\equiv 2.45E(V-I)/E(B-V)]$ is therefore 3.2 ± 0.1. This is slightly larger than the canonical value, $R = 3.1$.

The distance modulus of M11 can be determined from the distribution of the distance moduli of individual stars after correcting for interstellar reddening. In estimating $(V_0 - M_V)$ we used the ZAMS relation of Sung & Bessell (1999). The distribution of distance moduli shows a broad peak at $V_0 - M_V =$ 11.3–11.6, and a sharp drop at larger values. The ZAMS relation refers to the lower envelope of the MS band, but it is also affected by evolution and photometric errors. We took the distance modulus of M11 as $V_0 - M_V = 11.55$, the mean value of the last bin of the distance modulus distribution.

The distance moduli estimated from $(B-V,\ M_V)$ and from $(V-I, M_V)$ show a slight difference $[\Delta(V_0 - M_V) = 0.05 \pm 0.1]$. Such a small difference results from a slight difference in the ZAMS relation for late B-type stars, i.e. the bottom of the MS turn-off. In addition, evolution also affects this estimate because we used only bright stars ($V \leq 16$) in the cluster owing to the limitations of the proper motion study by MPS. The size of the evolutionary effects is very difficult to estimate, owing to a lack of information on the membership of fainter stars. We adopted the distance modulus of M11 as 11.55 ± 0.1 ($d = 2.0 \pm 0.1$ kpc). This value is consistent with that obtained by Kjeldsen & Frandsen (1991: $V_0 - M_V = 11.65 \pm 0.20$), but slightly larger than the distance derived by Johnson et al. (1956: $d = 1.66$ kpc). However Lee et al. (1989) obtained the lower limit of the *apparent* distance modulus of 12.7 (the best-fitting value is 12.8) by comparing the observed colour and magnitude of two spectroscopic binaries with the revised Yale isochrones. This value is well consistent with ours.

3.3 Radius of M11

The radius of a cluster can be determined from the surface density profile. Sung et al. (1996) determined a 10-arcmin radius for M11 from the surface density of blue stars in the $(B-V,\ V)$ CM diagram. But they observed only the central region of M11 using the same telescope at SSO and a SITe 2048×2048 CCD with high readout noise. In addition they divided the stars in the CM diagram into only two groups, and consequently the intermediate population dominated the cluster MS stars in the outer regions ($r > 10$ arcmin). Therefore they could find no noticeable variation in surface density at $r > 10$ arcmin. On the other hand, from the dynamical model calculations Mathieu (1984) estimated the tidal radius of M11 to be between 14 and 25 pc.

We have plotted the radial variation of the surface density of bright MS stars (group 1, see Section 4.1 for group division) in Fig. 8. In this figure, we used only bright stars ($V \leq 16$) to avoid the incompleteness of faint stars. The surface density decreases up to $r \sim 16$ arcmin as the radius increases, and beyond this the surface density becomes equal to that of field regions. We therefore adopt $r = 16$ arcmin (equivalent to 9.5 pc at $d = 2$ kpc) as the radius of M11. This value is somewhat smaller than the tidal radius obtained from the dynamical model calculations of Mathieu (1984), but larger than that derived by Sung et al. (1996).

3.4 Age

The age of a cluster is determined by comparing its CM diagram with theoretical isochrones. We have plotted the $(V,\ B-V)$ diagram in Fig. 9. The isochrones of the Padova group (Bertelli et al. 1994) in (a) and the Geneva group (Schaller et al. 1992) in (b) are superimposed. The small filled squares, open squares and crosses represent, respectively, proper motion members ($P_\mu \geq 0.7$), probable members ($0.5 \leq P_\mu < 0.7$), and non-members ($P_\mu < 0.5$). The large symbols denote the radial velocity members (filled) and non-members (open) from Mathieu et al. (1986). The broadening of the MS turn-off makes it difficult to assign a unique age to the cluster. Anthony-Twarog, Payne & Twarog (1989) interpreted the broadening at the MS turn-off as resulting from an age spread of about 7×10^7 yr. However, such a large age spread in an isolated cluster is difficult to accept because it is too large relative to the observed age spread in young open clusters (Massey, Johnson & DeGioia-Eastwood 1995; Sung, Bessell & Lee 1997, Sung et al. 1998).

There is another way to estimate the age spread in a cluster such as M11 with many red giants. The position of red giants in the CM diagram is very sensitive to the age of the cluster. In Fig. 9(a), it is seen that the position of most of the red giants is very consistent

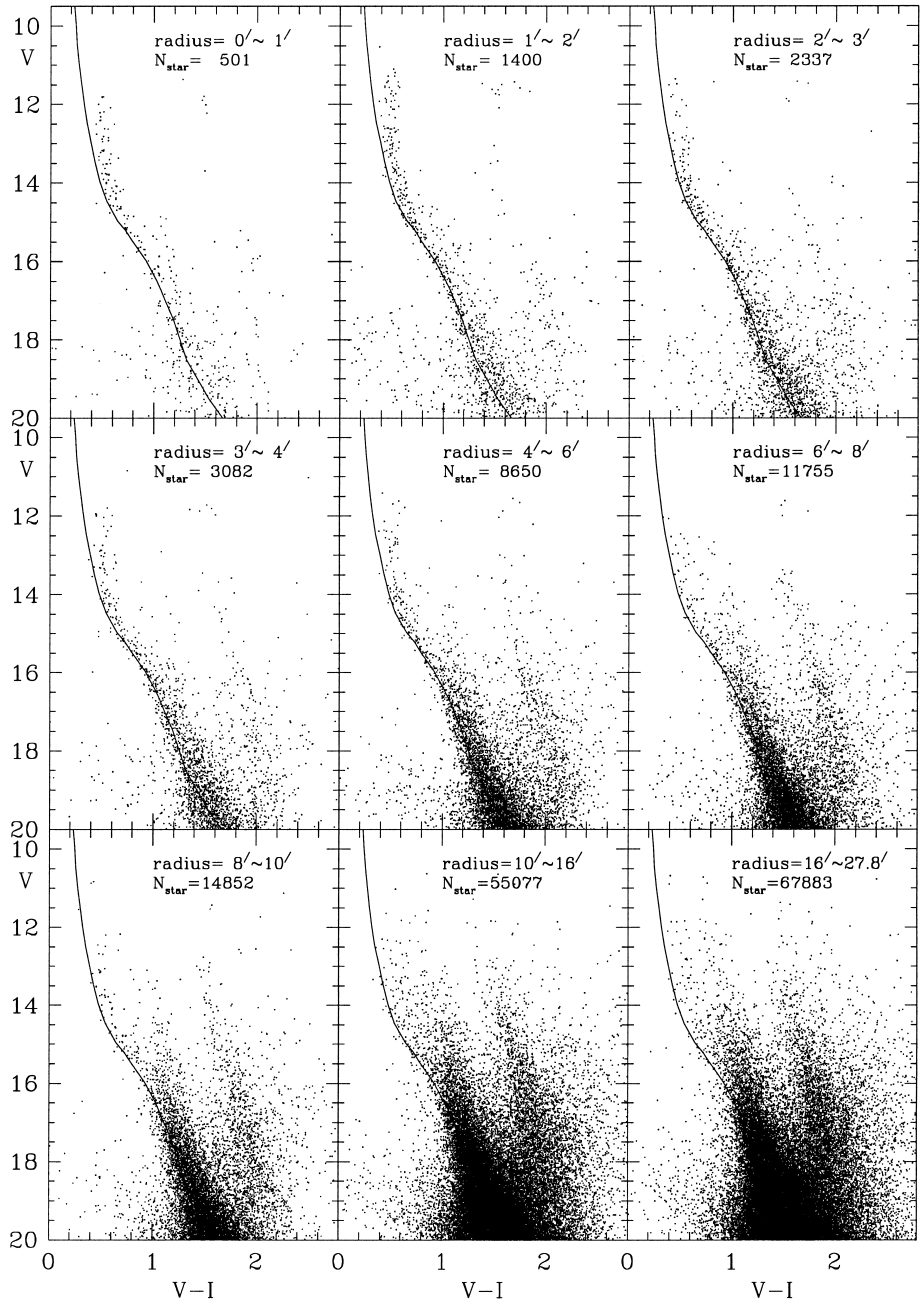

Figure 7. Radial variation of CM diagrams.

with the blue loop of the isochrones of ages between 8.3 and 8.4. On the other hand, the Geneva models (Fig. 9b) predict a slightly higher age, $\log t_{\rm age} = 8.4$–8.5. As can be seen in the figure, the isochrones from the Padova group give slightly brighter MS loci by about 0.2 mag relative to the empirical ZAMS at $(B-V)_0 = 0.2$, while those from the Geneva group are slightly fainter by about 0.1 mag. The youngest Padova isochrone ($\log t_{\rm age} = 6.6$) gives a MS locus slightly brighter by about 0.1 mag. In addition, the Geneva models predict a somewhat redder colour and brighter magnitude for the red giant locus for a given age. Such a colour discrepancy has already been mentioned by Mermilliod et al. (1996) for NGC 2099. Recently, Twarog, Anthony-Twarog & Ashman (1999) found a similar discrepancy from the comparison of the Sun's colour and magnitude with those predicted from these two isochrones of $Z = 0.02$. They also tried to zero the $Z = 0.008$ models using *Hipparcos* data and photometrically metal-deficient stars ([Fe/H] $= -0.4 \pm 0.1$) in the solar neighbourhood. If we take into account these differences in the ZAMS relations, the age of M11 is $\log t_{\rm age} = 8.45 \pm 0.05$ from the Geneva models and $\log t_{\rm age} = 8.35 \pm 0.05$ from the Padova models. Even if we adjust the MS line from the Padova models to the empirical ZAMS line at $(B-V)_0 = 0.2$, the age from the Padova model is close to $\log t_{\rm age} = 8.3$. The age of M11 determined from the theoretical isochrones is $\log t_{\rm age} = 8.4 \pm 0.1$.

In Fig. 9, three giant members are shown in the Hertzsprung gap (MPS 926, 1223 and 1364). Two giants, MPS 926 and 1223, are known spectroscopic binaries (Mathieu et al. 1986). Mathieu has suggested the multiplicity of MPS 1364 (Lee et al. 1989), but it

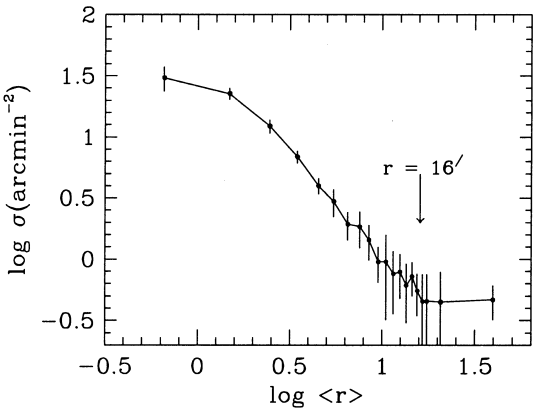

Figure 8. Radial variation of the surface density of bright stars, $V = 11$–16. The radius of M11 is ~16 arcmin as marked in the figure.

has not yet been confirmed. The proper motion membership of MPS 1364 is very high (0.99: MPS; 1.00: Su et al. 1998) and its radial velocity is $31.5 \pm 0.9\,\mathrm{km\,s^{-1}}$ (Mathieu et al. 1986). This value is about $2\sigma_{v_r}$ smaller than the cluster mean radial velocity ($\langle v_r \rangle = 34.5 \pm 1.4\,\mathrm{km\,s^{-1}}$).

4 SURFACE DENSITY PROFILE

4.1 Observed surface density profile

Mathieu (1984) found a group of field stars near the red end of the M11 MS band in the CM diagram. Sung et al. (1996) also noted the existence of such a group of stars. They divided the stars in the $(B-V, V)$ diagram into two groups and analysed the surface density of each group. The surface density of blue stars showed evident central enhancement, whilst for the red stars only the brightest magnitude bin (i.e. red giants of M11) showed a central

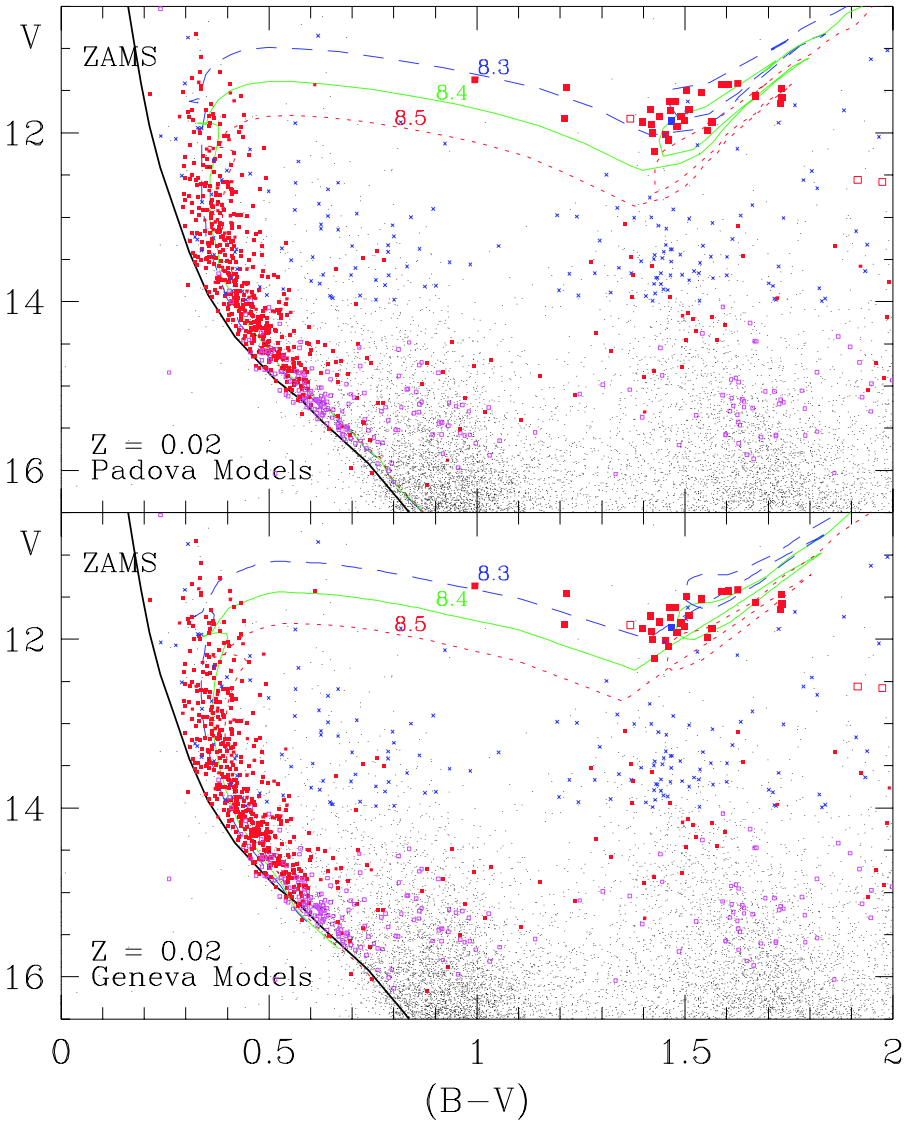

Figure 9. The age of M11. (a) The superimposed isochrones are taken from Bertelli et al. (1994). The filled squares, open squares and crosses represent, respectively, proper motion members ($P_\mu \geq 0.7$), probable members ($0.7 > P_\mu \geq 0.5$) and non-members ($P_\mu < 0.5$). The large filled squares and open squares are the radial velocity members and non-members. The dots denote stars without proper motion membership probabilities. (b) The superimposed isochrones are taken from the Geneva group (Schaller et al. 1992).

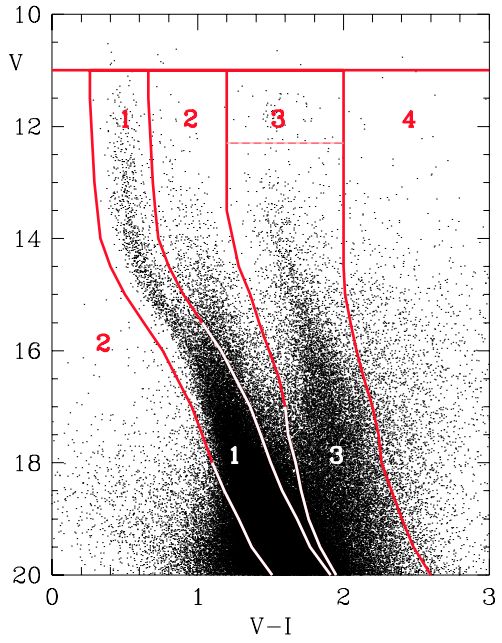

Figure 10. The schematic representation of group division for the surface density analysis.

enhancement. However, the intermediate population (bona fide field stars) were contributing to the surface density of blue stars, and hence they found no noticeable enhancement of cluster stars at larger radii ($r > 10$ arcmin).

For the surface density analysis, we have divided the stars in the CM diagram into four groups (Fig. 10). Group 1 is the MS stars of M11. To take into account the larger photometric errors for fainter stars and the broadening of the MS band near the MS turn-off, all stars within 0.2 mag in $(V - I)$ with respect to the mean line of the MS band are considered as group 1. Group 2 contains the field stars in the the red part of the MS band of M11, and other MS stars outside the MS band of M11. Group 3 comprises the red giant population, including the red giants of M11. Group 4 consists of the reddest stars in the CM diagram. They are probably field stars in the red giant branch or in the asymptotic giant branch, but we will pay no more attention to the group 4 stars, bona fide field stars in this paper.

All the known red giant members of M11 are brighter than $V = 12.3$. To include all the red giants of M11, we take the magnitude range of the brightest bin to be $V = 11$–12.3 (thin dashed line in Fig. 10). The bin size of the next brightest bin is, therefore, 0.7. For all other cases the bin size is 1. The surface density of each annulus relative to the cluster centre is calculated. The width of each annulus is 1 arcmin and the calculated centre (the ensemble average of $\Delta\alpha$ and $\Delta\delta$ of stars brighter than $V = 16$

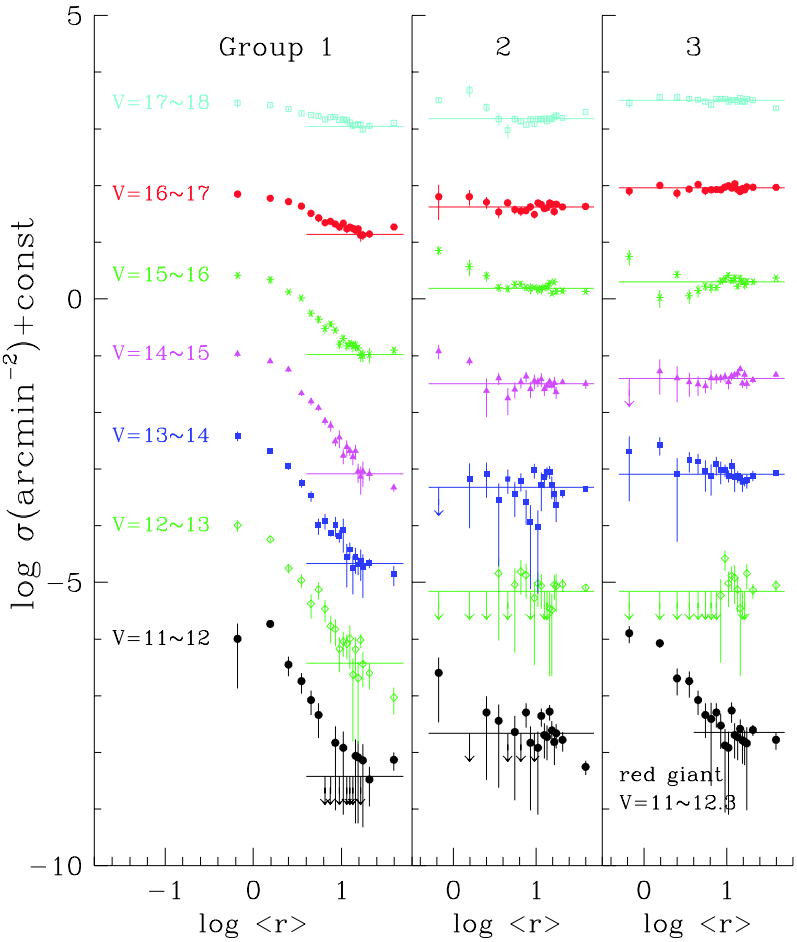

Figure 11. The observed surface density profile of three groups of stars. The downward-pointing arrows represent regions with no stars in the ring for a given magnitude bin. The horizontal lines represent the surface density of field stars. The stars in group 1 and the brightest stars in group 3 show a central enhancement of surface density.

in the central 3-arcmin radius) is 0.035 arcmin east and 0.198 arcmin north of the apparent centre (see Section 2). To calculate the error of the surface density, each annulus is divided into four sectors for the inner two rings ($r \leq 2$ arcmin) and eight sectors for the outer rings. The mean radius $\langle r \rangle$ is the ensemble mean value for $V < 18$.

Table 6 and Fig. 11 present the observed surface density profile of each group for M11. The points plotted as downward-pointing arrows only show the cases of no star in the bin. The surface density at the Scutum star cloud (PN G027.4−03.5) is included in the figure, but the values were not used in the calculation of the surface density of field stars, for two reasons. On the one hand, the region is far away from the cluster centre and hence may be affected differently by the irregular distribution of reddening material or field stars in the foreground or background, even though it is within the theoretical tidal radius ($r_t = 14$–25 pc: Mathieu 1984). On the other hand, the region was observed under bright moonlight and therefore the limiting magnitude is brighter by about 1 mag. In addition, it is a well-known fact that DAOPHOT gives brighter magnitudes for fainter stars, and hence the surface density of fainter stars may be slightly greater than the actual values. The horizontal lines in the figure represent the surface density of the field region ($r > 16$ arcmin).

Group 1 stars show an evident central enhancement in the surface density plot, while only the brightest bin of group 3 (red giants of M11) shows a distinct radial variation. Group 2 and the other magnitude bins of group 3 show no systematic radial variation of surface density. This fact strongly indicates that they are bona fide field stars, and confirms our previous thoughts. However, as already noted by Mathieu (1984, see his fig. 5), there is a small central enhancement of group 2 stars at fainter magnitudes ($V > 14$). This seems to be related to the increase in photometric errors owing to crowding in the central region.

4.2 Completeness test

4.2.1 Model cluster

The surface density of the fainter stars of group 2 shows a slight central enhancement. It is likely that such an apparent density enhancement of field stars can result from photometric errors in crowded regions. The central concentration of M11 is very high and therefore the crowding of stars affects the photometric error as well as causing faint stars to be missed. The presence of the very bright foreground star (star #2142 according to the adopted numbering system of (WE)BDA, the open cluster data base: Mermilliod 1995) near the centre of M11 may also strongly affect the completeness of the data. The V magnitude and $(B - V)$ of the star are about 8.5 and 0.65, respectively from Sung et al. (1996). In addition, M11 is located in a field of many foreground and background stars, namely the Scutum star cloud. To estimate the effect of crowding on the completeness and on the photometric precision, we performed a completeness test.

In most cases, completeness tests are performed by adding a few per cent of artificial stars to the original images. In those cases the number of added stars is very limited because the image quality should not be affected by the added stars. In M11, as mentioned above, a few per cent of added stars may easily affect the image quality. More than 50 000 stars can be found in a 1-min-exposure I image, and the situation is much more severe in the central region. Another way of testing the completeness is to construct a model cluster. In this case, the density structure of the real cluster will be preserved. To test the completeness of the data, we chose the second method.

To construct a model cluster, we simulated a blank CCD image with readout noise, and then added the sky brightness estimated from the sky value of a relatively blank area of the real images. After that we simulated the distribution of stars using the observed surface density profile up to $V = 22$. In the cluster simulation, the position, magnitude and $(V - I)$ colour of artificial stars were obtained using the Monte Carlo method. The colour of an artificial star was allowed to scatter along the mean CM relation of each group. No spatial density variation was considered for the field stars and the faintest MS stars ($V \geq 20$). For faint cluster MS stars ($V = 18$–20), a two- or three-step variation of surface density was considered. For stars with magnitude $V = 14$–18, the observed surface density of the central region was used, after taking into account the enhancement in the surface density of group 2 stars. The observed surface density was used for bright stars after smoothing the density profile. M11 is not a core-collapsed cluster, and therefore the surface density at the very centre should be finite. The density of the very centre was used by extrapolating the density to $\log r = -1$ in the $\log r$–$\log \sigma$ plane. In addition, the brightest star near the cluster centre was also included at the same distance from the cluster centre. After several tests, we finally adopted the model cluster 'ct4' in the completeness test of M11 (Fig. 12).

4.2.2 Completeness

A total of 148 739 stars were generated up to $r = 15$ arcmin but 72 032 stars fell within the 2048×2048 CCD image. Two sets (long and short) of V and I images were made using the PSF obtained on 1997 August 10 (long) and 1997 June 5 (short). Fig. 12 is the simulated 2048×2048 CCD image. From 72 032 added stars, 50 087 stars were recovered. Most of the missing stars were very faint, but some bright stars, especially in the central region, were missed because of merging with the brighter stars. The added and recovered CM diagrams are compared in Fig. 13. From the figure, we can easily see that the width of the MS band was broadened, especially for the faint stars, and the finding probability of faint red stars is better than that of blue stars owing to the high signal-to-noise ratio in the I images.

To see the completeness of the data quantitatively, we draw the radial dependence of completeness for each magnitude bin in Fig. 14. As expected, the completeness is strongly affected by crowding. The completeness of the whole sample is better than 99 per cent for the stars brighter than $V = 18$, but in the central region ($r \leq 1$ arcmin) it is about 86 per cent for $V = 17$–18. This result is better than expected. To see more of the effects of crowding, we plotted the magnitude and colour differences between input and output magnitudes for three typical rings in Fig. 15. For faint stars, the output magnitude is systematically brighter than the input magnitude, but the difference in the $(V - I)$ colour is less severe. At least the mean colour differences are close to zero down to $V = 20$. The magnitude differences in the $V = 17$–18 bin are -0.057 in V, -0.037 in I and -0.011 in $(V - I)$ in the innermost ring. Those for the second ring are less than half those of the innermost ring, while for the other rings the differences are less than -0.015 in the $V = 17$–18 bin. This

Table 6. Observed surface density.[a]

radius[b] / mag	0.665	1.559	2.510	3.519	4.517	5.515	6.512	7.516	8.506	9.503	10.502	11.506	12.504	13.505	14.502	15.506	16.503	17.498	20.746	39.4
											group 1									
11–12	1.273	2.334	0.446	0.227	0.106	0.058	0.000	0.000	0.019	0.000	0.015	0.000	0.000	0.000	0.011	0.010	0.000	0.009	0.042	0.009
	1.103	0.352	0.167	0.090	0.048	0.035	…	…	0.018	…	0.014	…	…	…	0.010	0.010	…	0.009	0.003	0.003
12–13	5.093	2.865	0.891	0.546	0.212	0.376	0.171	0.085	0.085	0.034	0.046	0.042	0.051	0.012	0.033	0.010	0.048	0.018	0.013	0.005
	1.191	0.231	0.174	0.144	0.097	0.129	0.073	0.042	0.037	0.021	0.021	0.019	0.036	0.011	0.022	0.010	0.013	0.011	0.006	0.002
13–14	7.639	4.138	2.228	1.137	0.672	0.203	0.245	0.149	0.206	0.134	0.167	0.055	0.076	0.035	0.055	0.041	0.048	0.036	0.044	0.028
	1.424	0.276	0.311	0.198	0.141	0.064	0.076	0.020	0.079	0.034	0.100	0.039	0.024	0.023	0.027	0.015	0.027	0.026	0.008	0.011
14–15	8.594	6.366	4.520	1.728	1.238	0.955	0.563	0.467	0.243	0.285	0.136	0.194	0.166	0.130	0.165	0.072	0.058	0.073	0.065	0.037
	1.137	0.475	0.387	0.179	0.187	0.112	0.088	0.103	0.045	0.099	0.040	0.061	0.031	0.037	0.050	0.027	0.030	0.034	0.016	0.006
15–16	8.276	6.897	4.202	3.274	1.768	1.389	0.955	1.146	0.899	0.503	0.637	0.471	0.522	0.472	0.483	0.431	0.318	0.327	0.331	0.395
	0.955	1.044	0.357	0.302	0.217	0.228	0.185	0.140	0.096	0.091	0.115	0.083	0.081	0.103	0.099	0.056	0.075	0.083	0.099	0.054
16–17	8.913	7.533	6.557	5.457	4.067	3.386	2.791	2.950	2.640	2.345	2.744	2.173	2.330	2.205	2.053	2.167	1.678	1.692	1.760	2.344
	1.191	0.988	0.472	0.572	0.466	0.554	0.256	0.342	0.161	0.331	0.359	0.333	0.241	0.246	0.283	0.322	0.399	0.300	0.263	0.129
17–18	14.324	13.157	11.205	9.504	8.736	8.479	7.370	8.106	8.126	7.187	7.382	7.100	6.545	5.718	5.905	6.027	5.836	4.893	5.692	6.397
	2.355	0.961	0.737	0.784	0.535	0.760	0.660	0.548	0.558	0.187	0.573	0.611	0.574	0.656	0.718	0.739	0.779	0.673	0.762	0.379
											group 2									
11–12	0.318	0.000	0.064	0.046	0.000	0.029	0.000	0.064	0.019	0.000	0.015	0.055	0.026	0.024	0.066	0.031	0.019	0.027	0.021	0.007
	0.276	…	0.060	0.043	…	0.027	…	0.029	0.018	…	0.014	0.020	0.016	0.014	0.021	0.014	0.012	0.013	0.008	0.002
12–13	0.000	0.000	0.000	0.046	0.000	0.029	0.049	0.042	0.000	0.017	0.030	0.028	0.000	0.000	0.011	0.010	0.029	0.027	0.029	0.026
	…	…	…	0.043	…	0.027	0.030	0.026	…	0.016	0.019	0.017	…	…	0.010	0.010	0.013	0.018	0.008	0.004
13–14	0.000	0.106	0.127	0.046	0.106	0.058	0.098	0.042	0.019	0.151	0.015	0.083	0.115	0.142	0.143	0.082	0.058	0.036	0.059	0.070
	…	0.092	0.078	0.043	0.048	0.035	0.035	0.026	0.018	0.044	0.014	0.055	0.042	0.029	0.038	0.036	0.023	0.018	0.009	0.002
14–15	0.955	0.637	0.191	0.318	0.142	0.203	0.269	0.340	0.206	0.285	0.273	0.305	0.204	0.236	0.274	0.236	0.260	0.182	0.272	0.252
	0.276	0.106	0.125	0.077	0.071	0.063	0.059	0.074	0.065	0.084	0.051	0.083	0.048	0.037	0.039	0.027	0.077	0.045	0.019	0.048
15–16	2.865	1.485	1.019	0.637	0.601	0.723	0.735	0.637	0.618	0.637	0.591	0.595	0.649	0.648	0.757	0.503	0.801	0.546	0.553	0.540
	0.528	0.486	0.201	0.107	0.093	0.112	0.096	0.084	0.141	0.052	0.112	0.116	0.054	0.107	0.096	0.049	0.068	0.082	0.057	0.019
16–17	1.273	1.273	1.019	0.682	0.993	0.752	0.710	0.722	0.843	0.620	0.985	0.927	0.789	0.814	0.988	0.934	0.695	0.937	0.839	0.855
	0.780	0.397	0.238	0.150	0.123	0.128	0.134	0.084	0.127	0.098	0.133	0.083	0.091	0.103	0.093	0.139	0.109	0.051	0.027	0.017
17–18	3.183	4.775	2.419	1.501	0.955	1.505	1.371	1.188	1.461	1.223	1.501	1.467	1.515	1.379	1.515	1.499	1.611	1.737	1.565	1.991
	0.318	1.156	0.420	0.383	0.283	0.220	0.193	0.095	0.158	0.149	0.121	0.145	0.077	0.113	0.148	0.181	0.125	0.213	0.078	0.059

Table 6 – *continued*

radius[b] / mag	0.665	1.559	2.510	3.519	4.517	5.515	6.512	7.516	8.506	9.503	10.502	11.506	12.504	13.505	14.502	15.506	16.503	17.498	20.746	39.4
											group 3									
11–12.3	1.592	1.061	0.255	0.227	0.106	0.058	0.049	0.064	0.037	0.017	0.015	0.069	0.026	0.024	0.033	0.021	0.019	0.018	0.031	0.021
	0.528	0.184	0.127	0.110	0.048	0.035	0.046	0.029	0.023	0.016	0.014	0.027	0.016	0.014	0.015	0.013	0.012	0.017	0.007	0.007
12.3–13	0.000	0.000	0.000	0.000	0.000	0.000	0.000	0.000	0.019	0.084	0.030	0.042	0.038	0.024	0.011	0.000	0.000	0.045	0.023	0.028
	…	…	…	…	…	…	…	…	0.018	0.033	0.019	0.019	0.025	0.014	0.010	…	…	0.022	0.007	0.007
13–14	0.318	0.424	0.127	0.227	0.212	0.145	0.122	0.191	0.150	0.151	0.121	0.180	0.115	0.118	0.110	0.092	0.097	0.100	0.121	0.138
	0.276	0.150	0.119	0.090	0.083	0.081	0.069	0.070	0.065	0.037	0.030	0.059	0.052	0.028	0.021	0.031	0.018	0.029	0.025	0.011
14–15	0.000	0.424	0.318	0.273	0.248	0.232	0.318	0.318	0.318	0.335	0.273	0.346	0.369	0.389	0.461	0.257	0.367	0.255	0.295	0.365
	…	0.260	0.200	0.124	0.093	0.058	0.120	0.063	0.056	0.067	0.070	0.057	0.036	0.072	0.040	0.042	0.074	0.050	0.039	0.035
15–16	2.228	0.424	1.082	0.455	0.566	0.666	0.637	0.637	0.824	0.888	1.046	0.844	0.930	0.672	0.922	0.811	0.714	0.809	0.802	0.940
	0.694	0.150	0.167	0.125	0.142	0.112	0.128	0.072	0.121	0.128	0.111	0.100	0.145	0.084	0.158	0.081	0.135	0.135	0.092	0.056
16–17	1.592	2.016	1.464	1.728	2.087	1.621	1.690	1.698	1.685	1.876	1.986	1.813	2.152	1.709	1.570	1.766	1.688	1.901	1.865	1.861
	0.276	0.176	0.291	0.247	0.283	0.265	0.213	0.124	0.152	0.200	0.157	0.192	0.234	0.208	0.176	0.184	0.179	0.198	0.168	0.033
17–18	2.865	3.607	3.629	3.411	3.289	3.038	2.669	3.374	3.352	3.401	3.047	3.225	3.234	3.018	3.480	3.080	3.038	3.401	3.196	2.307
	0.528	0.486	0.521	0.401	0.300	0.296	0.323	0.176	0.196	0.286	0.267	0.264	0.164	0.210	0.375	0.261	0.262	0.242	0.220	0.168

[a] The first row of each magnitude bin represents the observed surface density in units of arcmin^{-2}. The second row is the standard error of the surface density.
[b] Mean radius (in units of arcmin) of stars brighter than $V = 18$.

means that the completeness of data for $V < 18$ at $r > 2$ arcmin is very good.

4.2.3 *Effect on the surface density*

The large fluctuations between the input and output data imply that crowding may have some severe effects on the surface density profile. This phenomenon is related to the broadening of the MS band in Fig. 13. To estimate the effect due to crowding on the surface density profile, we used the same surface density analysis as in the previous section. We have drawn the input and output surface densities for groups 1 and 2 in Fig. 16. For brighter stars ($V \leq 14$) the crowding does not affect the measured surface density, but differences occur at $V \approx 14$. The output surface density of the inner region is reduced for group 1, but increased for group 2. However, for fainter stars in the outer region

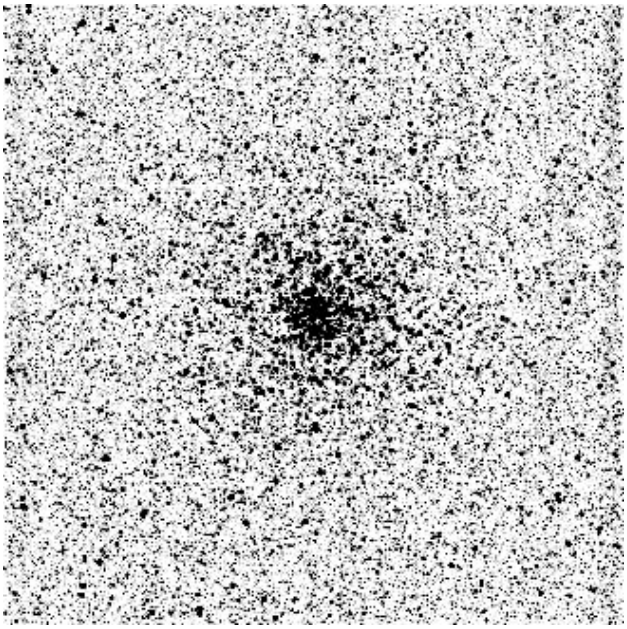

Figure 12. The model cluster 'ct4' constructed for the completeness test. A total of 72 032 artificial stars were added for the image.

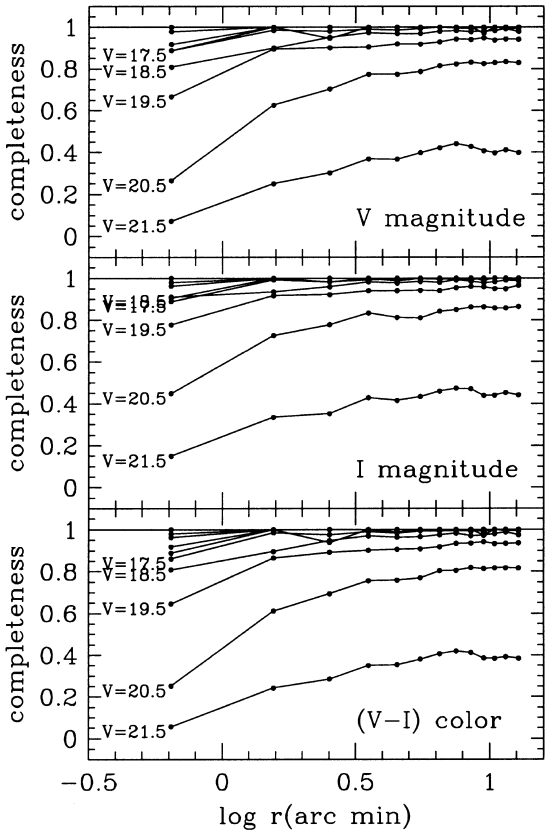

Figure 14. The radial dependence of completeness. The completeness at the cluster centre is very low relative to the outer region.

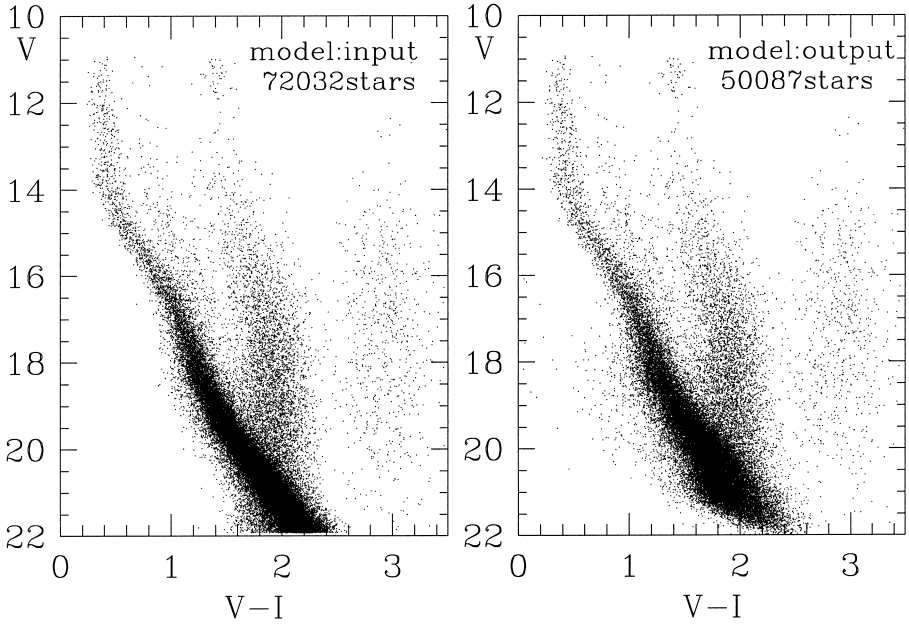

Figure 13. The CM diagrams from the model cluster. The left panel represents the input CM diagram. The right panel represents the resulting output CM diagram. The broadening of each sequence and the loss of faint stars can be seen clearly.

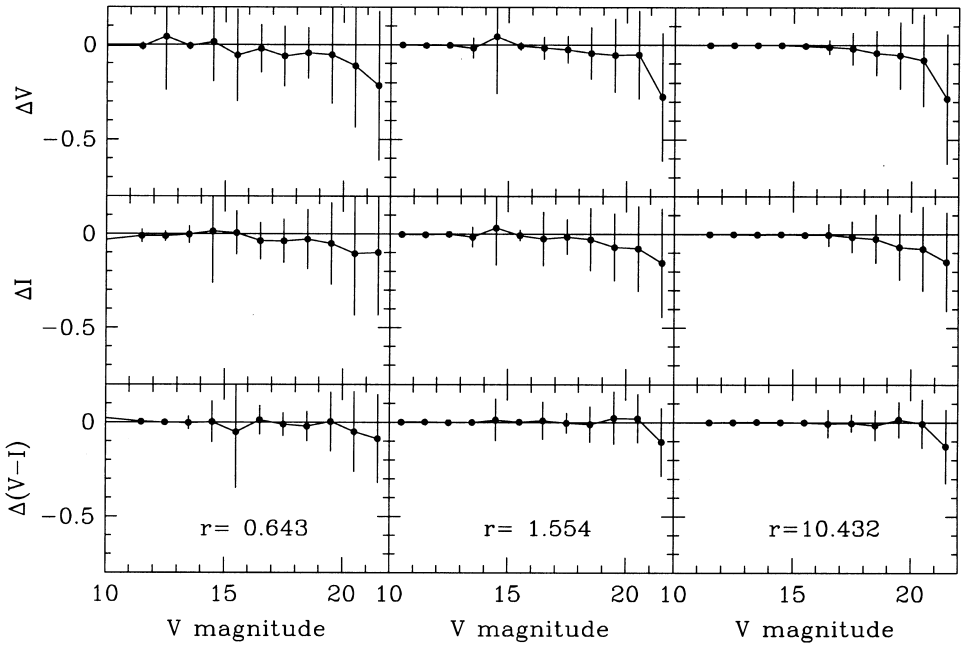

Figure 15. The magnitude difference in the sense of output magnitude minus input magnitude of V, I and $(V-I)$ for three typical rings. The output magnitude is systematically brighter for the fainter regime. The fluctuations are evidently affected by the crowding, i.e. the standard deviation at a given magnitude is larger at the centre but smaller in the outer regions.

($r > 2$ arcmin), the surface densities increase for both groups 1 and 2. This was an unexpected result and may be caused by the brightening effect of fainter stars. More numerous fainter stars ($V > 18$) were measured as too bright, and therefore the surface density of the faintest bin increased.

The actual completeness can be calculated from the surface density analysis. For brighter stars ($V < 14$) the completeness of the data is nearly perfect and there is no need to apply the completeness correction. The actual completenesses of the innermost ring ($r \leq 1$ arcmin) are 88 per cent for $V = 14$–15, 84 per cent for 15–16, 88 per cent for 16–17, and 77 per cent for 17–18. Those for the other rings are better than 95 per cent.

4.3 Cluster surface density profile

4.3.1 Surface density of field stars

The surface density of cluster stars can be obtained by subtracting the field star contribution. For groups 2, 3 (except the brightest bin) and 4, the field star contribution can be easily obtained from the average surface density of the whole area, but the crowding in the central region may over- or underestimate the actual surface density. For fainter stars ($V > 14$), the inner rings were neglected in the calculation of mean surface density.

An estimation of the field star contribution to the MS (group 1) and to the red giants (the brightest magnitude bin of group 3) is difficult. For MS turn-off stars, the surface density of stars in the field region, as well as in the outer cluster region, is too low. There are many rings having no stars in the range $V = 11$–12. The field star contribution in group 1 was estimated at $r > 12$ arcmin for the brightest bin, at $r > 13$ arcmin for $V = 12$–13, at $r > 15$ arcmin for $V = 13$–14, and at $r > 16$ arcmin for the other magnitude bins ($V > 14$). However, the surface density of the Scutum star cloud (PN G027.4−03.5) was not taken into account owing to probable differences in the surface density with respect to the field region of M11. The difference can be easily seen in Fig. 11. The field

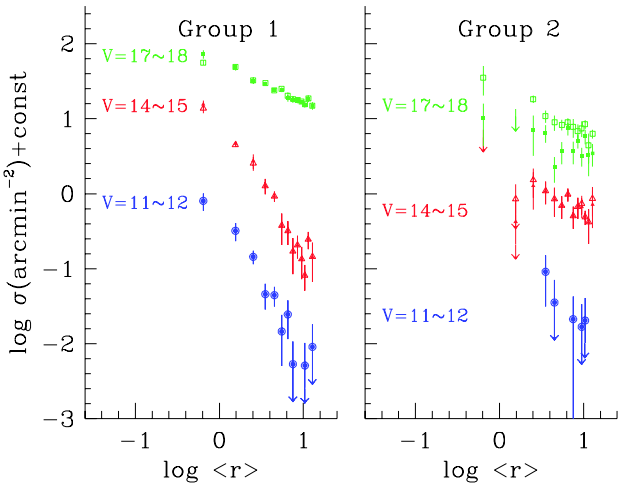

Figure 16. The effect of crowding on the surface density. Filled symbols represent the input surface density, while open symbols denote the output surface density. The surface density of bright stars is not affected by the crowding. That of fainter stars ($V \geq 14$) is strongly affected by the crowding. At the centre, the surface density of group 1 is reduced, while that of group 2 is increased. In the outer region, the surface density is increased independently of the stellar group.

contribution of red giants was calculated from the same regions as that of the MS turn-off. The derived cluster surface density is listed in Table 7 and plotted in Fig. 17. The left panel of the figure shows the radial variation of the surface density without any completeness correction, while on the right is plotted the same surface density profile with the field contribution subtracted and after correcting for incompleteness. For bright stars, the two distributions are the same, but the surface density of faint stars in the inner region is increased slightly. The field star contribution is also listed in the last column of the table.

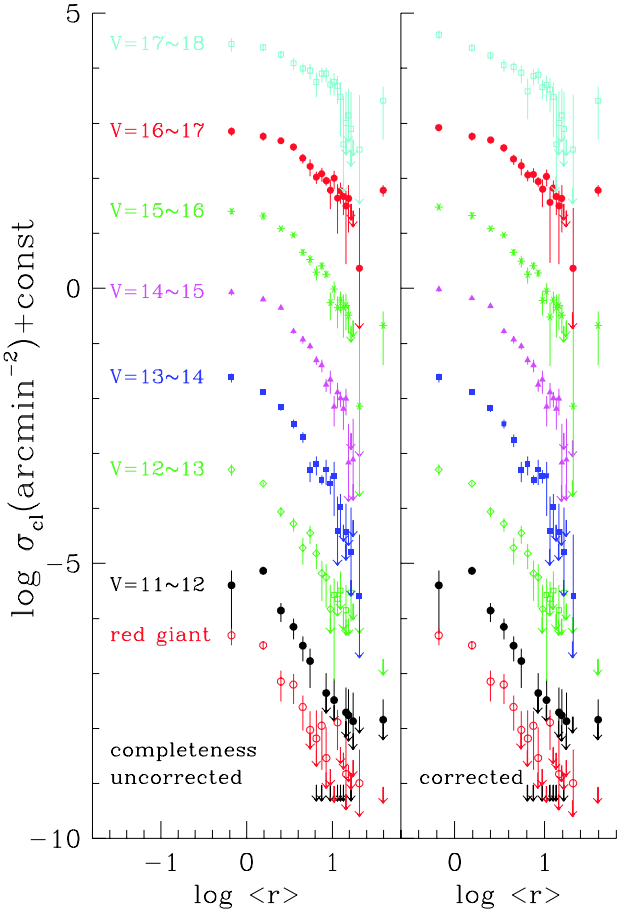

Figure 17. The surface density profile of the cluster M11. The panel on the left represents the cluster surface density uncorrected for completeness, while on the right it is corrected for incompleteness. The downward-pointing arrows without data points denote data with non-zero upper limits, while the downward-pointing arrows with data points denote data with negative values of the lower limit.

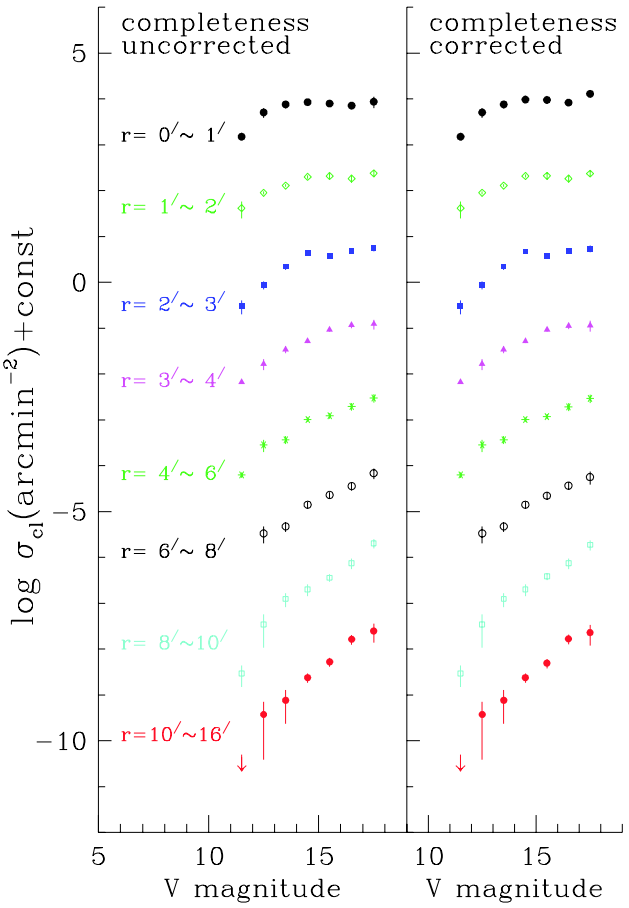

Figure 18. The differential luminosity function at various radii. The luminosity at the centre is evidently flatter than that of the outer regions.

Mathieu (1984) pointed out that the radial distribution of red giants shows a marginal difference relative to that of MS turn-off stars. Sung et al. (1996) also demonstrated their different radial distribution. Our new results, however, show no difference in radial distribution for these two groups. Such a difference may have been caused by a difference in the field star contribution. The surface density of MS turn-off stars in the field region is $0.005\,\mathrm{arcmin}^{-2}$, while that of the red giants is $0.028\,\mathrm{arcmin}^{-2}$. A factor of more than 5 difference in the field star density could cause such a difference in the radial distribution from a limited sample. In the PN G027.4−03.5 region, nine red giants and four MS stars were found. The red-to-blue ratio is smaller than that in the field region of M11, but such bright stars are very rare and highly dependent on the spatial region. Sung et al. (1996) used 1-mag bins in their data analysis. In that case a few faint red giants were missed and therefore they may have underestimated the red giant density.

4.3.2 *Luminosity function and mass function*

The cluster luminosity function at different radii is plotted in Fig. 18. In the outer region, the surface density of bright stars is too low. The widths of the annuli used in the luminosity function calculation were 1 arcmin in the inner region ($r \leq 4$ arcmin), 2 arcmin in the $r = 4$–10 arcmin region, and 6 arcmin for the outer region. The surface densities of red giants and of MS turn-off stars were merged because of their having similar masses. The slope of the luminosity function increases as the radius increases. Because the most massive stars (MS turn-off and red giant) are very narrow in mass range, there is an abrupt drop in the luminosity function at the bright end. As noted above, the completeness correction does not much affect the slope of the luminosity function in the faint regime.

The currently accepted dynamical models predict a mass segregation owing to equipartition of kinetic energy amongst cluster members, via two-body encounters. The age of M11 is about 2.5×10^8 yr, which is greater than its relaxation time ($\tau_{\mathrm{relax}} = 4 \times 10^7$–$1.3 \times 10^8$ yr: Mathieu 1984). Mass segregation may already have been achieved in M11. To see any mass segregation effects more clearly, we have plotted the differential mass function at various radii in Fig. 19. In the transformation from luminosity function to mass function, we used the mass–luminosity function for the Padova isochrone of age $\log t_{\mathrm{age}} = 8.3$ in order to include the brightest stars in the cluster. A small increase at the most massive bin was caused by the small mass range of the evolved stars, and is not used in the calculation of the slope. The slope of the mass function Γ is defined as $\mathrm{d}\log\xi(\log m)/\mathrm{d}\log m$. The Γ of the solar neighbourhood is

Table 7. Cluster surface density.[a]

radius / mag	0.665	1.559	2.510	3.519	4.517	5.515	6.512	7.516	8.506	9.503	10.502	11.506	12.504	13.505	14.502	15.506	field
	1.563	1.033	0.226	0.199	0.078	0.030	0.021	0.036	0.009	−0.011	−0.013	0.041	−0.003	−0.005	0.005	−0.008	0.028
red giant	0.528	0.184	0.128	0.110	0.049	0.036	0.046	0.030	0.024	0.017	0.016	0.028	0.017	0.016	0.017	0.015	0.007
	1.268	2.330	0.441	0.223	0.101	0.053	−0.005	−0.005	0.014	−0.005	0.010	−0.005	−0.005	−0.005	0.006	0.006	0.005
11–12	1.103	0.352	0.167	0.090	0.049	0.036	0.005	0.005	0.018	0.005	0.015	0.005	0.005	0.005	0.012	0.011	0.005
	5.074	2.846	0.873	0.527	0.194	0.358	0.153	0.066	0.056	0.015	0.027	0.023	0.032	−0.007	0.014	−0.008	0.019
12–13	1.191	0.232	0.175	0.145	0.098	0.130	0.075	0.045	0.041	0.026	0.026	0.025	0.039	0.019	0.027	0.018	0.016
	7.596	4.095	2.185	1.094	0.629	0.160	0.202	0.105	0.163	0.091	0.124	0.012	0.033	−0.008	0.012	−0.002	0.043
13–14	1.424	0.276	0.311	0.198	0.141	0.064	0.076	0.021	0.079	0.034	0.101	0.039	0.024	0.024	0.027	0.015	0.005
	8.529	6.301	4.455	1.663	1.173	0.890	0.498	0.402	0.178	0.220	0.071	0.129	0.100	0.065	0.100	0.007	0.065
14–15	1.137	0.475	0.387	0.179	0.187	0.112	0.088	0.103	0.046	0.099	0.040	0.062	0.032	0.038	0.051	0.028	0.008
	9.728	6.605	4.794	1.663	1.173	0.890	0.498	0.402	0.178	0.220	0.071	0.129	0.100	0.064	0.100	0.007	
	7.948	6.568	3.873	2.946	1.440	1.061	0.627	0.818	0.571	0.174	0.308	0.142	0.194	0.143	0.155	0.103	0.328
15–16	0.955	1.044	0.357	0.302	0.217	0.228	0.185	0.140	0.096	0.091	0.115	0.083	0.082	0.103	0.100	0.056	0.007
	9.557	6.701	3.873	2.946	1.440	0.988	0.572	0.818	0.602	0.192	0.279	0.095	0.194	0.143	0.155	0.103	
	7.176	5.797	4.820	3.720	2.331	1.649	1.055	1.213	0.903	0.609	1.007	0.436	0.593	0.468	0.316	0.430	1.737
16–17	1.192	0.990	0.475	0.574	0.470	0.556	0.262	0.346	0.170	0.335	0.363	0.337	0.247	0.252	0.288	0.326	0.055
	8.353	5.797	4.980	3.585	2.243	1.693	1.152	1.178	0.875	0.636	1.081	0.366	0.664	0.468	0.316	0.430	
	8.737	7.570	5.618	3.917	3.149	2.892	1.784	2.520	2.540	1.601	1.795	1.513	0.958	0.131	0.319	0.441	5.587
17–18	2.413	1.096	0.906	0.944	0.751	0.925	0.844	0.760	0.768	0.559	0.778	0.806	0.779	0.841	0.891	0.907	0.527
	12.970	7.456	5.443	3.628	3.356	2.619	1.217	2.294	2.404	1.431	1.564	1.301	0.958	0.131	0.319	0.441	

[a] The first row of each magnitude bin represents the field-subtracted observed surface density. The second row is the standard error of the first row. The third row for $V = 14$–18 is the completeness-corrected cluster surface density.

-1.35 (Salpeter 1955). We used the median mass in the figure, and the slope may be slightly underestimated.

The slope of the mass function increases systematically as the radius increases. The completeness correction of the data only affects the slope at the innermost ring. To show the variation of mass function slope, we have drawn the slope Γ as a function of radius in Fig. 20. The slope of the mass function at large radii is clearly steeper and far greater than that of the solar neighbourhood. Similar results were obtained for the Pleiades and Praesepe by Raboud & Mermilliod (1998a,b). The slope of the mass function of the inner part of the Pleiades (the Hertzsprung region) is $\Gamma = -0.7 \pm 0.14$, while that of the outer halo is $\Gamma = -2.2 \pm 0.16$. Similar values were obtained for the Praesepe cluster ($\Gamma = -0.6 \pm 0.4$ in the inner region, -2.6 ± 0.7 in the outer region). Owing to the small size of the sample in the Pleiades and Praesepe, Raboud & Mermilliod divided them into only two regions.

4.3.3 Total luminosity and mass functions

The total luminosity function of M11 was obtained by directly summing the products of surface density and spatial coverage. The total mass function was also derived in the usual way, $\xi(\log m)\,\mathrm{d}\log m = \psi(M_V)\,\mathrm{d}M_V$, and is shown in Fig. 21. The calculated slope of the mass function is shown in the figure. The derived slope ($\Gamma = -2.3 \pm 0.5$ excluding the most massive stellar bin; -2.0 ± 0.6 from all points) is somewhat steep relative to that of the solar neighbourhood or of the Pleiades or Praesepe ($\Gamma = -1.5 \pm 0.3$: Raboud & Mermilliod 1998a,b).

The steep slope is entirely caused by the enhancement of the faintest two bins. This is related to the estimation of the field star contribution. We derived the surface density of field stars in the outer regions at the adopted radius ($r_{\mathrm{M11}} = 16$ arcmin: see Section 3.3). The surface density of faint stars ($V = 16$–18) in the outer rings is evidently higher than that of the field region. There are two possible explanations. One is that it is due to underestimation of the cluster radius. In order to avoid large photometric errors and the incompleteness of the faint star data, we derived the cluster radius from the surface density variation of relatively bright stars, $V = 11$–16. If we underestimated the actual cluster size, the slope of the MS stars might be steeper. The other possibility is that it is due to the spatial surface density variation of field stars. This is highly probable. In the northern part of M11 ($\Delta\delta > 12$ arcmin), the surface density of faint stars ($V < 15.5$) is very low; the surface density in the southern part is also slightly low. This may be caused by an irregular distribution of obscuring material.

5 DISCUSSION

5.1 Red stars

One distinct feature in the CM diagrams (see Fig. 3) is the red stars that are fainter than the M11 giants. As already mentioned in Section 3.1, their colours imply that most of them are red giants, but they are well extended in magnitude down to $V \approx 19$ (see also fig. 5 of Brocato et al. 1993). Brocato et al. mentioned the possible relationship between the group of stars at $V \approx 16.5$ and $(B - V) \approx 1.0$ (the intermediate population: the brighter part of the group 2 stars) and the red star population. Sung et al. (1996) also suggested that they might be disc giant stars in the Sgr–Car arm. To check these suggestions, we have drawn the $(V - I, V)$ diagram again in Fig. 22. The fiducial line of M67 from Montgomery, Marschall & Janes (1993) and the position of clump stars in M67 at the distance and reddening of M11 are superimposed (solid line). In addition, a reddening vector of $E(V - I) = 0.6$ and the isochrone of age 8 Gyr ($Z = 0.02$) are plotted as thick solid and dotted lines, respectively. The clump stars of age 8 Gyr and those in M67 (4 Gyr) are very similar. From the white dwarf luminosity function, Liebert, Dahn & Monet (1988) derived an age for the disc of between 7 and 10 Gyr. So it is likely that the majority of stars in the disc will lie between these two loci.

M11, with galactic coordinates (27.3, -2.8), lies near the tangent to the Sgr–Car arm. It is a complicated region, as shown by IR scans in Hammersley et al. (1994), where stellar contributions from an exponential disc, the Sagittarius arm, the Scutum arm and possibly the end of the 3-kpc bar can be identified. However, Hammersley et al. find smooth profiles indicating low and/or uniform extinction. Also, being $2\overset{\circ}{.}8$ below the plane, the line of sight to M11 lies away from the maximum extinction. There is a further complication in that old H I maps have been interpreted as indicating a spur extending from the Sun across to the Sgr arm in the direction of M11 as well. So one might expect there to be stars at all distances in front of and beyond M11.

The wide branch in Fig. 22 (and Fig. 4) to the right of the MS could be explained as MS stars near the turn-off with a range of ages (about 4 to 8 Gyr), a range of reddenings (0.3–0.6 mag) and a range of distances (1 to 5 kpc). If this is correct, then we would expect there to be associated red giants about 0.5 mag redder in $(B - V)$ and $(V - I)$ and up to 2 mag brighter in V. Perhaps we can identify the red stars that are fainter than the M11 giants as such stars. However, at first glance we would have expected a composite red giant branch corresponding to such a wide composite MS to be much wider than it appears to be. One explanation could be that the bulk of the stars are red clump stars that have similar temperatures for a range of masses, and so when such stars with a range of ages, distances and reddenings are combined they trace out a narrow locus in the CM diagram.

We intend in a future paper to model such scenarios using theoretical cluster luminosity functions derived from the evolutionary tracks of Bressan et al. (1993). We also plan to make follow-up photometric observations in the DDO system to get more detailed information on these red stars.

6 SUMMARY

Extensive *UBVI* CCD photometric data have been obtained for the intermediate-age open cluster M11. The results obtained are summarized as follows.

(1) The distance and mean reddening $E(B - V)$ of the cluster are 11.55 ± 0.1 ($d = 2.0 \pm 0.1$ kpc) and 0.428 ± 0.027, respectively. The total-to-selective extinction ratio $R = 3.2 \pm 0.1$ has been derived from the colour excess ratio $E(V - I)/E(B - V)$.

(2) The radius of $r = 16$ arcmin ($R = 9.5$ pc at $d = 2$ kpc) has been determined from the surface density profile of bright stars ($V = 11$–16). This value is smaller than the theoretical tidal radius ($r_{\mathrm{t}} = 14$–25 pc).

(3) The age of M11 has been derived from the theoretical isochrones of the Padova and Geneva groups. The age of the cluster derived by matching the locus of red giants is ($\log t_{\mathrm{age}} = 8.4 \pm 0.1$).

(4) The surface density profiles for three groups of stars have

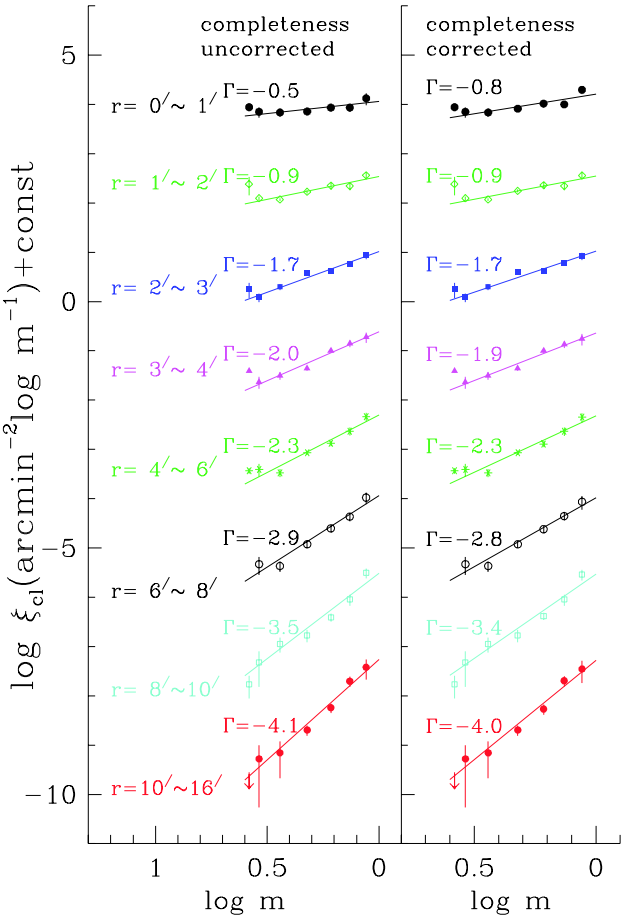

Figure 19. The differential mass function at various radii. The relation $\xi(\log m, r)\,\mathrm{d}\log m \equiv \sigma(M_V, r)\,\mathrm{d}M_V$ was used in the mass function calculation. The mass–luminosity relation for the isochrone of age $\log t_{\rm age} = 8.3$ from the Padova group was used. The slope of the mass function $\Gamma(\equiv \mathrm{d}\log\xi(\log m)/\mathrm{d}\log m)$ was calculated using six points (excluding the most massive bin). The slope of the mass function increases systematically as the radius increases.

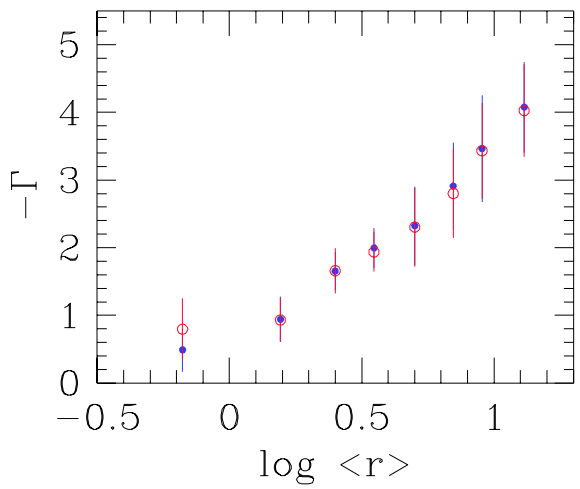

Figure 20. The radial variation of the mass function slope. The filled symbols represent the slope calculated from the incompleteness-uncorrected data, while the open symbols denote the slope from incompleteness-corrected data. The completeness correction affects the slope at the cluster centre; however, the trend of systematic variation of the slope is lessened, but not changed.

been derived and presented. Only the MS stars and the brightest red giants show an obvious central enhancement. The bright stars are more centrally concentrated, while the faint stars are more widely distributed.

(5) Using a Monte Carlo technique, we have constructed a model cluster with a similar surface density profile, and performed completeness tests. The results show that the faint stars ($V > 14$) in the innermost region are strongly affected by crowding. On the other hand, the surface density of faint stars in the outer region increases slightly owing to the brightening of faint stars in the photometric reduction procedure. In addition, the crowding of stars affects the precision of the photometry. We believe that the slight enhancement in the surface density of bona fide field stars is an artificial effect.

(6) The luminosity function and mass function of M11 show a marked difference between the inner and outer regions. The slope of the mass function systematically steepens as the distance from the centre increases, i.e. mass segregation has already been achieved in M11.

(7) Red giants fainter than $V = 12.5$ are a field population possibly made up of old disc clump stars extending from 1 to

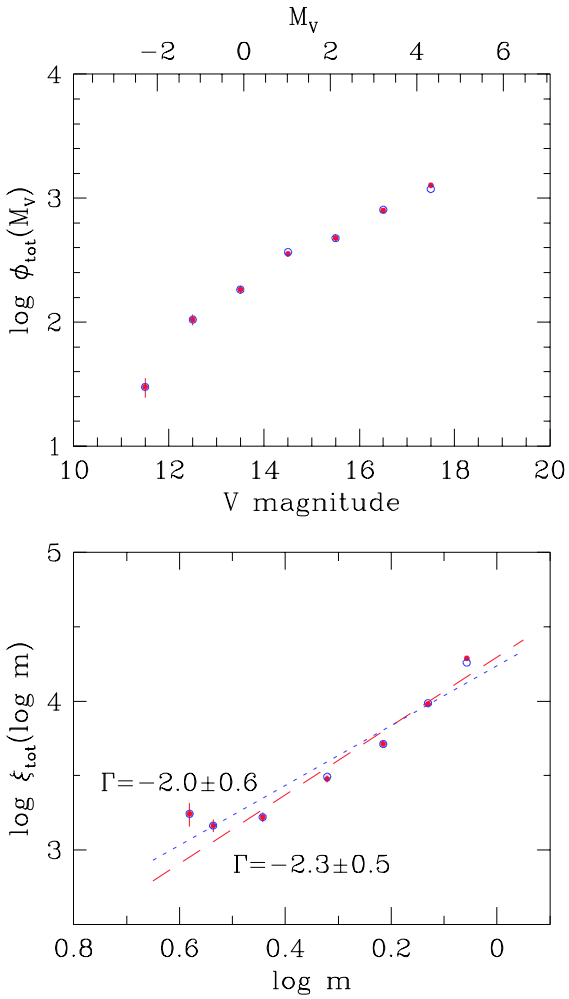

Figure 21. The total luminosity and mass functions. The enhancement of low-mass stars may be caused by field subtraction owing to the large-scale variation of the field star density.

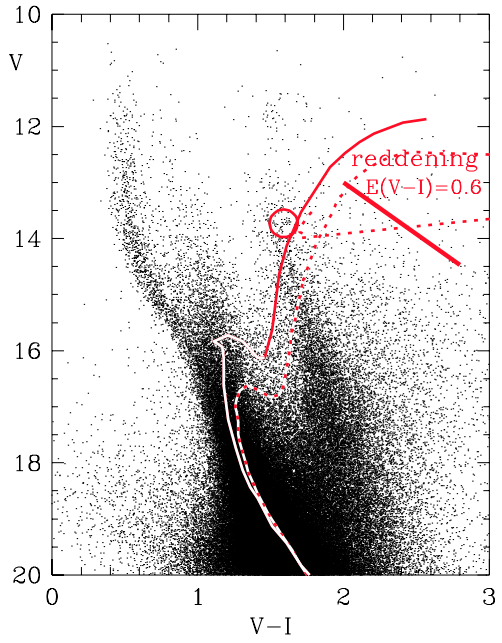

Figure 22. The CM diagram with, superimposed, the fiducial line and the clump star position of M67 at the distance and reddening of M11. The dotted line represents the isochrone of age 8 Gyr at the distance and reddening of M11. The thick line is the reddening vector for $E(V-I)=0.6$.

5 kpc. Corresponding precursor main-sequence stars are probably those stars to the right of the M11 main sequence.

ACKNOWLEDGMENTS

HS and H-WL acknowledge the support of the Kyungpook National University's Post-Doc Program. S-WL acknowledges the support of the Korea Science and Engineering Foundation, Grant KOSEF (95-0702-01-01-3). The authors express deep thanks to the referee, Dr B. J. Anthony-Twarog, for helpful comments and many suggestions.

REFERENCES

Anthony-Twarog B. J., Payne D. M., Twarog B. A., 1989, AJ, 97, 1048
Bertelli G., Bressan A., Chiosi C., Fagotto F., Nasi E., 1994, A&AS, 106, 275
Bessell M. S., 1995, PASP, 107, 672
Blaauw A., 1963, in Strand K. E., ed., Star and Stellar Systems, Vol. 2, Basic Astronomical Data. Univ. Chicago Press, Chicago, p. 383
Bressan A., Fagotto F., Bertelli G., Chiosi C., 1993, A&AS, 100, 647
Brocato E., Castellani V., DiGiorgio A., 1993, AJ, 105, 2192
Cousins A. W. J., 1978, Mon. Not. Astron. Soc. S. Afr., 37, 62
Eggen O. J., 1974, PASP, 86, 129
Guetter H. H., Vrba F. J., 1989, AJ, 98, 611
Hammersley P. L., Garzón F., Mahoney T., Calbet X., 1994, MNRAS, 269, 753
Harris G. L. H., 1976, ApJS, 30, 451
Johnson H. L., Sandage A. R., Wahlquist H. D., 1956, ApJ, 124, 81
Kilkenny D., van Wyk F., Roberts G., Marang F., Cooper D., 1998, MNRAS, 294, 93
Kjeldsen H., Frandsen S., 1991, A&AS, 87, 119
Lee C. W., Mathieu R. D., Latham D. W., 1989, AJ, 97, 1710
Liebert J., Dahn C. C., Monet D. G., 1988, ApJ, 332, 891
McNamara B., Sanders W. L., 1977, A&A, 54, 569
McNamara B., Pratt N. M., Sanders W. L., 1977, A&AS, 27, 117 (MPS)
Massey P., Johnson K. E., DeGioia-Eastwood K., 1995, ApJ, 454, 151
Mathieu R. D., 1984, ApJ, 284, 643
Mathieu R. D., Latham D. W., Griffin R. F., Gunn J. E., 1986, AJ, 92, 1100
Menzies J. W., Cousins A. W. J., Banfield R. M., Laing J. D., 1989, SAAO Circ., 13, 1
Menzies J. W., Marang F., Laing J. D., Coulson I. M., Engelbrecht C. A., 1991, MNRAS, 248, 642
Mermilliod J.-C., 1981, A&A, 97, 235
Mermilliod J.-C., 1995, in Egret D., Albrecht M., eds, Information & On-Line Data in Astronomy. Kluwer, Dordrecht, p. 127
Mermilliod J.-C., Huestamandia G., de Rio G., Mayor M., 1996, A&A, 307, 80
Montgomery K. A., Marschall L. A., Janes K. A., 1993, AJ, 106, 181
Perryman M. A. C. et al., 1998, A&A, 331, 81
Raboud D., Mermilliod J.-C., 1998a, A&A, 329, 101
Raboud D., Mermilliod J.-C., 1998b, A&A, 333, 897
Sagar R., Myakutin V. I., Piskunov A. E., Dluzhnevskaya O. B., 1988, MNRAS, 234, 831
Salpeter E. E., 1955, ApJ, 121, 161
Schaller G., Schaerer D., Meynet G., Maeder A., 1992, A&AS, 96, 269
Schmidt E. G., 1984, ApJS, 55, 455
Schmidt-Kaler K., 1982, Landolt–Börnstein, Vol. 2b, pp. 19, 453
Solomon S. J., McNamara B. J., 1980, AJ, 85, 432
Sowell J. R., 1987, ApJS, 64, 241
Stetson P. B., 1991, PASP, 102, 932
Stetson P. B., Harris W. E., 1988, AJ, 96, 909
Su C.-G., Zhao J.-L., Tian K.-P., 1998, A&AS, 128, 255
Sung H., Bessell M. S., 1999, MNRAS, 306, 361
Sung H., Lee S.-W., Lee M. G., Ann H. B., 1996, J. Korean Astron. Soc., 29, 269 (Paper I)
Sung H., Bessell M. S., Lee S.-W., 1997, AJ, 114, 2644
Sung H., Bessell M. S., Lee S.-W., 1998, AJ, 115, 734
Twarog B. A., Ashman K. M., Anthony-Twarog B. J., 1997, AJ, 114, 2556
Twarog B. A., Anthony-Twarog B. J., Ashman K. M., 1999, AJ, 117, 1816

This paper has been typeset from a TEX/LATEX file prepared by the author.